Modeling NO and CO Emissions in Lean Natural Gas Spark Ignition Engines

by

Aaron D. Golub

B.S. Mechanical Engineering
Virginia Polytechnic Institute and State University, 1994

Submitted to the Department of Mechanical Engineering
in Partial Fulfillment of The Requirements for the Degree of

Master of Science in Mechanical Engineering

at the

Massachusetts Institute of Technology

August, 1996

Signature of Author: _____
Department of Mechanical Engineering
August, 1996

Certified by: _____
Ahmed F. Ghoniem
Professor of Mechanical Engineering
Thesis Supervisor

Accepted by: _____
Ain A. Sonin
Professor of Mechanical Engineering
Chairman, Departmental Graduate Committee

Modeling NO and CO Emissions in Lean Natural Gas Spark Ignition Engines

by

Aaron D. Golub

Submitted to the Department of Mechanical Engineering
in Partial Fulfillment of the Requirements for the Degree of
Master of Science in Mechanical Engineering

Abstract

Legislation limiting NO_x and CO emissions from production natural gas engines dictate a need for greater understanding of the mechanisms governing these pollutants' formation. This work concerns the formulation of a one dimensional, multizoned, thermochemical model incorporating detailed kinetics for calculating NO and CO emissions from small, lean burning natural gas engines.

The model calculates the temperature and pressure histories for each part of the working fluid throughout the combustion, compression and expansion phases. The gradients in the burned gases' properties resulting from the finite combustion time are maintained by the segmentation of the product field. The burn rate is input as either an harmonic function approximating standard burn rates or a burn rate discretized from experimental measurements. Because of the potential for significant non equilibrium effects from the lean operation, high engine speeds and small combustion chamber sizes, full kinetic mechanisms are used to integrate the reaction rates over the duration of the product segments' histories. The bulk gas properties are calculated at the end of every crank angle via an energy equation which balances the energy budget during that crank angle.

The model is used to predict NO emissions from experimental engines over a small range of lean conditions: $\phi = 0.91$ and $\phi = 0.66$. The richer case is more easily modeled than the leaner cases and further investigation into this difference helps to illuminate the dominant mechanisms for NO formation in these engines. The richer mixtures produce NO by processes which are formation limited in the colder, later burned region, and decomposition limited in the hotter, earlier burned region. In the lean engines, however, NO is formed solely via a formation limited process. The balanced process in the richer engines renders modeling easier as the calculations are not as sensitive to inputs as are the unbalanced lean conditions.

CO emissions in lean engines have been seen to result from flame quenching via wall interactions. Further experimental data is reviewed here to substantiate that observation and to emphasize the need for a quenching mechanism in any CO modeling effort. The lack of spatial dimension in the model leaves this phenomena hard to model and thus CO predictions using the fundamental model differ greatly from experiment. Adding a mechanism to approximate imperfect mixing helps to illustrate the possible significance it could have in real engine and combustor environments.

The advantages of building a model with detailed kinetic capabilities are not clear. Simplifying the kinetics via steady state and equilibrium assumptions were shown to be reasonable for most of the conditions explored in this work. The ease of incorporating detailed chemistry, however, can be useful to explore the significances of certain chemical reactions or rates or to test new fuels or additives theorized to control emissions levels.

Thesis Supervisor: **Dr. Ahmed Ghoniem**
Title: **Professor of Mechanical Engineering**

Acknowledgments

I owe much gratitude to my advisor, Dr. Ahmed Ghoniem, for his guidance over the past two years. I have learned much from and will always remember both our academic and 'extracurricular' discussions.

I must thank my officemates Adrin, Van, Costa, Issam and Jean-Pierre as well as Pat for their camaraderie and support during these interesting and sometimes grueling months.

I also give much thanks for the various friends I've made during my time here at MIT. First and foremost comes Jean-Claude, for all of our hours of studying and laughing. I couldn't have asked for a better partner during all of this. As well, come Nora, Sharon, Chris and Stephanie for making MIT and Boston a very memorable experience and my departure from it so saddening. Dealing with MIT and life in general during the past two years was made a little easier as well with my friend Amy.

Like always, my parents Thea and Elliott and my sister Jennifer were there for me during this work and for that I thank them and love them. (Cosette the cat, too.) It was undoubtedly their influence, along with that of my grandparents, which prepared me for this.

A more fundamental thanks must go to the hundreds of millions of working people the world over who's sweat and suffering have built the foundations for institutions like MIT and all of the wealth they embody.

My work at MIT was supported mainly by the National Science Foundation and the Gas Research Institute. Computer support was provided by the National Center for Supercomputing Applications at the University of Illinois.

Table of Contents

1. Background

1.1 Introduction

For millions of years, man has altered his environment in various ways in an effort to live and survive. As man's expertise and domain have grown, so has the extent to which he has altered his environment. Different technologies have emerged from the various challenges facing human progression as well as from the different forms human society has taken. A widespread and important era in the history of human development is the growth of the modem industrial society. It is characterized by a dense, built environment and a very concentrated mixture of both industry and human settlements. The concentrated nature of these settlements and industries causes large disturbances in the local environment, namely, the air, water, and soil, to the point of becoming dangerous to the heath and well being of their inhabitants, both animal and plant.

This work focuses on two particular air pollutants, NO and CO, and how they are formed in one of their common sources, the internal combustion engine. Ensuing regulation could place a limit on the level of these pollutants emitted by a range of small, natural gas engines. In this work, a model geared for these small, fast, natural gas burning engines with a focus on lean operation will be constructed to enable prediction of emissions levels of NO and CO. Different engine configurations and operating conditions will be tested and compared with experimental measurements. Mechanisms controlling CO and NO formation under lean operation and how different design changes might limit these pathways will be discussed. In working to meet emissions regulations, modeling like this helps reduce the number of tests needed to be run and helps to steer development efforts.

1.2 Thesis Organization

The rest of chapter 1 deals with a brief history of air pollution and some discussion of current pollution legislation. The important aspects of the two substances focused on in this work, NO and CO are described. Chapter 2 begins with an overview of the model which forms the backbone of

this work. Before constructing the model, a review of previous research in modeling emissions is given, highlighting important conclusions for this work. The rest of Chapter 2 is dedicated to constructing the model from first principles. The modeling of NO is discussed in Chapter 3 with comparisons to previous work and experimental results. In Chapter 4, the modeling of CO is discussed along with the various issues which make CO modeling difficult. Final conclusions with respect to engine combustion and emissions modeling are made in chapter 5.

1.3 Air Pollution: Brief History

From the moment fire was discovered roughly 1.4 million years ago [21], humans have changed the air they breath and affected both their own health as well as that of their immediate environment. Fire became important for cooking, forest clearance for farming, heating, making signals for communication, and light. At around 7000 BC, fire became central to metal refining and smelting in both Indochina and the Middle East. This introduced newer and more toxic pollutants like sulfur dioxide, lead, soot, and arsenic.

A significant change in the nature of air pollution came with the development of the steam engine in the middle 1700s. Now, humans could extract more of the earth's stored energy in more and diverse applications [18]. The development of the combustion driven engine, along with slavery and the plundering of the natural resources of the new world, brought the European capitalist class into greater wealth and control, steering the course of western civilization towards industrialization. Steam engines fueled mainly by coal drove machines for textiles manufacture, railroads, and mining and supplied the raw power in this push towards industrialization. This increased the intake of fuels and materials by orders of magnitude and so increased those effects these industrial centers had on the local environments. Charles Dickens described the typical British industrial town in his novel, Hard Times:

> "it was a town of machinery and tall chimneys, out of which interminable serpents of smoke trailed themselves for ever and ever, and never got uncoiled."[16]

This description could apply to any industrial city from Seattle to Bangkok. Urbanization grew with industrialization. In 1800 about 2.5% of the world's population lived in cities, but by the 1980s, the number had grown to 43%. In 1800 world coal consumption was about 15 million tons and by 1900, it had ballooned to 700 million tons. Although electricity, steam and petroleum were all prevalent among turn of the century automobile power plants, it would be for many reasons, both practical and political, that petroleum would become the fuel of choice. In 1890, shortly after

the invention of the automobile, 10 million tons of petroleum were consumed but by the 1970s that number reached over 2500 millions tons annually [16].

In the United States, where some of the world's worst urban air pollution exists, much of which is produced by cars, car and petroleum firms began intervening in the public transit sector early on. As early as the 1920's, street cars and other rail services were bought and dismantled in favor of greater car and bus access and more and wider streets. GM orchestrated most of these purchases in joint ventures with Chevron, Phillips Petroleum, Firestone Tire, and Mack Truck. In all, rail systems were disassembled in 85 US cities [35]. Car manufacturers even subsidized the building of car garages on the new wave of suburban single family home developments. By the 1950s, US automakers had constructed an entire 'car culture' in the wake of their efforts which would compound the problem of declining air quality of US cities.

The use of electric appliances and airplanes escalated during the mid 1900s and contributed to the effects large urban areas were having on the local and regional environment. The cities, originally built around industry, became criss-crossed by electric power lines, highways and roads and by the 1950s, dangerous levels of pollutants clouded the world's urban areas. Occasional smog 'events' occurred, where particular weather conditions would amplify the dangerous effects of the polluted air. In two weeks of heavy pollution in London during the winter of 1952-1953, more than four thousand people died from respiratory illnesses [36] Similar events have struck New York City, Osaka, Japan, and Donora, Pennsylvania.

Today, hundreds of millions of people breath dangerously polluted air. Heavily polluted cities, those that exceed the World Health Organization's (WHO) standards, span the globe. The most notorious are Mexico City, Tehran, Sao Poulo, Karachi, Bangkok, Seoul, Santiago, and Cairo, with a scattering of 'dirty' cities throughout the former Soviet Union, India, China and Eastern Europe. Residents of Los Angeles breathed air which failed WHO standards on 159 days during 1992. In Houston, it was 40 days, New York, 26 and in Washington D.C., 20. [17]

1.4 Reducing Urban Air Pollution

Legislation in the form of mandates like the Clean Air Act of 1970 and the Clean Air Bill of 1989 along with countless local air quality laws seek to reduce pollution levels through prevention or control. In response to the clean air act and other local laws, engine developers and manufacturers have sought out new designs, operating conditions and fuels in hopes of meeting current and future legislation. The small natural gas engine is used in a wide variety of applications and may

soon be included in emissions legislation. Both as a stationary and mobile source, limits on the NO_x, CO and unburned hydrocarbon emissions from natural gas engines may soon be mandated. Table 1.1 below compares a few mandates with typical range of emissions from small gas engines:

Table 1.1

Law	NO_x (ppm)	CO (ppm)
EPA - passenger car		
current	270	1420
post 1995	108	
California Air Resources Board - passenger car		
current	110	2840
Low Emissions	55	710-1420
SCAQMD[a]		
gas furnaces	103	
water heaters	103	
stationary or portable engines	102-153	
Typical Small Gas Engine at Lean Conditions	300-350	1120

a: South Coast Air Quality Management District (California)

One strategy for pollution reduction is operating the engine at lean conditions. The particular issues surrounding natural gas combustion as well as lean burn operation will be the focus of this modeling effort. Before the modeling is discussed, a brief introduction to the particular effects NO and CO have as air pollutants will be given.

1.5 Effects of Air Pollution

Polluted air is a general description for air which contains substances which are toxic or harmful in some way to the being (plant, animal, human) depending on that air for life. Polluted air to a Birch tree might not be polluted to a chimpanzee or a frog, or each may have different resilience to the same pollutant. The major air pollutants in the urban/suburban 'soup' are sulfur dioxide, nitrogen oxides (NO_x, i.e. NO + NO_2), carbon monoxide, hydrocarbons, ozone, peroxyacyl nitrates (PANs), and particulates like soot. This work concerns the formation of NO and CO and next we will take a closer look at why they are classified as pollutants.

1.5.1 Effects of NO

NO is harmful to both people and the environment for three basic reasons: it is directly toxic to humans and plants, it reacts with other compounds in the air to form harmful secondary pollutants, and it acidifies the water in the atmosphere which damages ecosystems sensitive to acidity.

The toxicity of NO to humans and laboratory animals has been widely established [14]. NO has been found, at even moderate levels, to constrict respiratory function and irritate asthmatics [14]. Further exposure leads to "sudden circulatory collapse or congestion and water accumulation in the lungs" [14, p74]. Chest pains are likely to become permanent in affected individuals. People exposed to moderate but extended levels can develop liver or kidney damage which can lead to permanent problems like Silo-Filler's Disease.

Much of the cause of concern about NO is its potential to form other more reactive and destructive secondary pollutants. The following illustration found in Wellburn [14] shows simply how NO interacts with light and O_3.

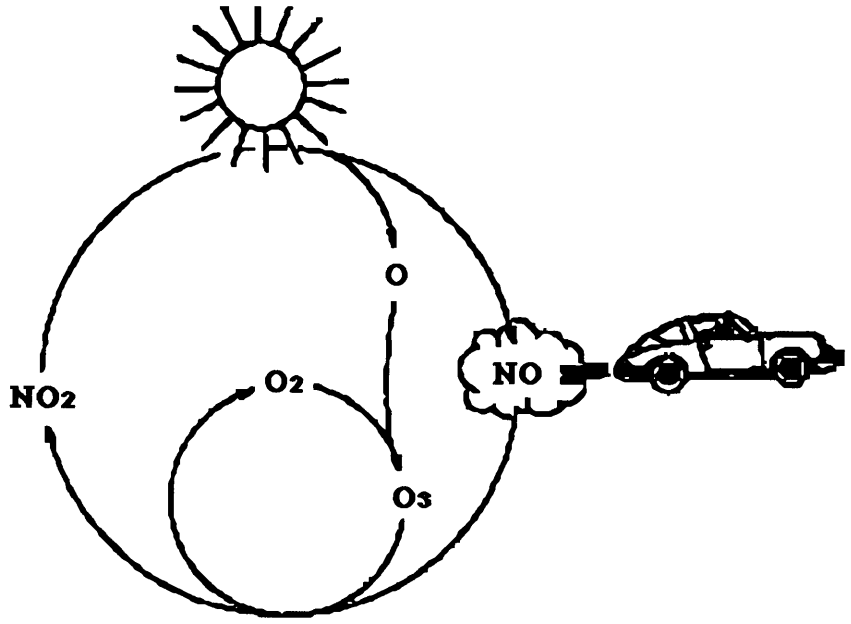

Figure 1.1. Atmospheric interactions among NO, O_3 and NO_2 from Wellburn [14,p123].

The proportions of O_3, NO_2, and NO in the air depend mainly on the level of irradiation and unburned hydrocarbons. Hydrocarbons produce free radicals under irradiation which later combine with the nitrogen oxides to form peroxyacyl nitrates (PANs). This soup of PANs, HC radicals, Ozone, NO and NO_2 is called photochemical smog.

The daily cycle of pollutant release and oxidation brings rise to a distinct pattern. Wellburn illustrates the general progression of a polluted atmosphere under typical radiation beginning with

the soup of emissions from a morning rush hour.

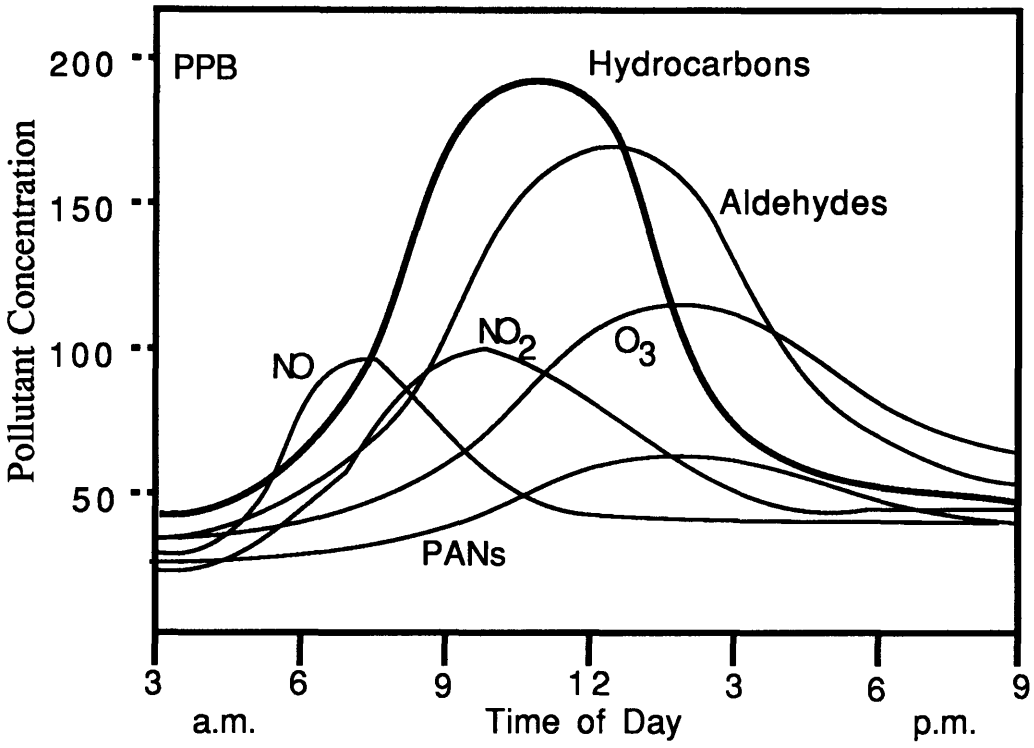

Figure 1.2. Typical progression of polluted atmosphere during a bright, warm and still day. [14, p126]

Both Ozone and PANs, because of their reactive nature, are destructive to living things. Tissue in plants and animals (lungs, nose, throat) are highly venerable to the oxidizing nature of these reactants and can experience serious damage. NO_2 is very dangerous to lung and bronchial tissue as well and affects the ability for the lung to defend itself against bacterial infection.

The pathways for nitric acid formation from nitrogen oxides in the atmosphere are complicated but can be summarized by either:

$$N_2O_5 + H_2O \rightarrow 2HNO_3$$

or

$$\bullet OH + NO_2 + M \rightarrow HNO_3 + M.$$

Nitric acid in cloud water precipitates out and affects the acidity of groundwater and soil. Nutrients

are leached by the added proton concentration which can effect soil fertility. Most common marine life can withstand only a narrow range of pH, beyond which streams and ponds become lifeless. The effects of acidity on fish is summarized in Wellburn below:

Table 1.2

pH range	Effect
6.5 - 9	No effect
5.0 - 6.4	Not likely to be harmful
4.5 - 4.9	Harmful to the eggs of Salmon and Trout species (salmanoids) and to adults when levels of Ca^{2+}, Na^{+}, and Cl^{-} are low.
4.0 - 4.4	Harmful to adult fish of many types with no low pH acclimation
3.5 - 3.9	Lethal to Salmanoids
3.0 - 3.4	Most fish are killed within hours at these levels

Table adapted from Wellburn, p.116

1.5.2 Effects of CO

CO is directly toxic to humans by its extreme effect on the blood's ability to uptake oxygen. Blood Haemoglobin's affinity for CO is between 2 and 3 *hundred* times that for O_2, which can have enormous affects on the body's ability to operate. At only 600 ppm inhaled CO, 50% of the oxygen carrying capacity of the blood is compromised. A summary of the effects of CO on the body is given below:

Table 1.3

Exposure (ppm)	COHB/HB[a] (%)	Effects
10-50	2-10	Tiredness, reduction in manual dexterity
50-100	10-20	Slight headache, tiredness and irritability
100-200	20-30	Mild headache
200-400	30-40	Severe headache, visual impairment, nausea, weakness
400-600	40-50	Increased possibility of collapse
600-800	50-60	Increased pulse rate and convulsions
800-1600	60-70	Coma, weak pulse and possibility of death
>1600	>70	Death imminent

a. Percentage of blood Heamoglobin (HB) occupied by COHB.
Table adapted from Wellburn, p.200

2. The COOK Model

2.1 Introduction

The goal of any emissions model is to predict the concentrations of pollutants in the exhaust. To make this prediction most accurately, one would calculate the complex mechanics of the swirling and highly turbulent in-cylinder fluid motion, the propagation of the reaction zone, the reactions and mixing among the products, and other phenomena like heat transfer, crevice and oil layer interactions, spontaneous ignition sites and flame quenching. These calculations would give the thermo-mechanical history (Pressure, temperature and strain rate) of every portion of the working fluid making it possible to calculate accurately the changing chemistry of the mixture, given a highly accurate and detailed chemical mechanism.

Modeling, in essence, is evaluating the aspects of the phenomena which have the greatest influence on what one hopes to calculate. The amount of the overall physics kept in the model is dependent upon the level of accuracy desired and the computational power available for the calculation. Some models are purely chemical, others incorporate with the chemistry a one dimensional thermodynamic model of the engine. Others divide the products into zones (still one dimensional) or add geometric conveniences for the in situ calculation of the flame propagation. The most advanced solve for the three dimensional flow field but correspondingly are hindered in their chemical accuracy because of the limits on the computational power.

The model called Cook, the basis of this work, is multizoned zero-dimensional and will be formulated step by step later in this chapter. The emphasis in constructing COOK is on modeling lean engines burning natural gas. COOk's formulation is based loosely on the conditions which it might be dealing with in lean, natural gas engines, specifically, but not limited to:

1. The possibility of low temperatures and low pressures

2. High engine speeds

3. Small cylinder size.

These factors might influence both the thermochemical aspects of the engine's operation as well as the way in which different aspects of the phenomena should be modeled fundamentally. Many of the particular issues to modeling both NO and CO emissions will be addressed in chapters 3 and 4, respectively. In addressing the general issues mentioned above, it was decided that COOK should need to incorporate detailed chemistry, since high speeds and leaner operation could make equilibrium and steady state assumptions harder to justify a priory. Under fast and lean operation chemical time scales might become closer to other governing time scales like changing pressures and temperature and this would facilitate the need for more accurate chemistry than in a richer slower environment. In this way, COOK differs from other emissions models, most of which have simple kinetic calculations for the pollutants under investigation, while leaving the rest of the C-H-O system alone under an equilibrium assumption.

In the next sections, COOK will be formulated from first principles. Before doing so, however, an investigation into previous works is made to help illuminate useful assumptions and conclusions for emissions modeling arrived to by earlier researchers.

2.2 Previous Work in Emissions Modeling

Beginning with fundamental chemical studies and proceeding to more complex engine cycle calculations, past modeling work has become more and more robust. Here, a review of the major work done in the modeling of emissions from spark ignited engines will be useful in formulating the present study. While the focus of this work is only on small, lean burning, natural gas engines, these models can give valuable insight into the broad issues involved in modeling emissions.

Of fundamental importance to any model of NO and CO emissions are the kinetics of NO formation and CO oxidation. Zeldovich delineated much of the thermal NO formation kinetics which form the basis for the accepted mechanism. Here, nitrogen and oxygen in the air react with N and 0 radicals to form NO. Lavioe added a third reaction involving OH after further experimental engine work with NO formation.

Miller and Bowman summarize the Nitrogen chemistry in combustion and flames and emphasize the importance of NO formation via the thermal mechanism. The alternate 'prompt' mechanism which produces NO 'promptly' in the flame zone from reactions involving CH and CH2 is said to

be of little importance for the modeling of "clean" fuels' (those containing no nitrogen) combustion [26]. An N_2O route which is faster than the thermal (Zeldovich) mechanism but not part of the traditional prompt mechanism could also contribute to NO emissions and has been implicated to be of importance in methane combustion over a wide range of operating conditions [38]. Others show that the N_2O pathway is more important for rich combustion [39].

The most simple model of NO and CO emissions would be an equilibrium calculation of the fuel-air mixture at exhaust conditions. After some experimental work measuring NO levels in the engine [3], Newhall recognized that equilibrium calculated values were typically low by orders of magnitude in most cases. It was clear that CO oxidation and NO decomposition were kinetically impeded during the expansion phase, yielding higher than equilibrium values. He then did a calculation of both NO and CO kinetics during expansion which begin at peak pressure with an equilibrium mixture of combustion products and an approximate temperature-crank-angle relationship for the expansion. A set of 34 elementary reactions are then integrated along the expansion stroke and compared with their equilibrium values. His major conclusions are that NO decomposition is too slow and becomes quenched fairly early in the expansion stroke. CO oxidation becomes inhibited by an excess of H radicals. H and OH recombinations are slowed during expansion but not proportionally, yielding an excess of H with respect to OH. This excess of H forces the dominating CO oxidation reaction

$$CO + OH <--> CO_2 + H$$

to the left, inhibiting CO oxidation. Newhall's work clearly showed the importance of kinetics in any useful calculation of emissions.

The significance of post flame gradients in temperature and in NO concentration was introduced by Lavoie, et al [7]. This work combined experimental measurements with a one dimensional cycle simulation taking input burn rates from an experimental engine. The model is based on burn rates calculated from the pressure history of the engine, assuming constant specific heats and zero heat transfer. Two models of the burned gas regions were tested, a "mixed" and an "unmixed" one. The mixed case assumes the product zone is homogeneous and has no gradients in neither composition nor temperature. The unmixed model assumes the products are divided into separate segments according to when they are burned. The different sections do not transfer heat nor mass. The engine measurements included in the study show clear and substantial gradients in both temperature and NO concentration and verify the validity of the unmixed model. Flame-zone levels

of NO are seen to be minuscule and verify the lack of need to include the prompt NO mechanism in engine models. In all kinetic calculations, the C-H-O system was assumed to be in equilibrium and some radicals like N were assumed to be in steady state.

Using a more flexible burn rate calculated from harmonic functions, Blumberg and Kummer extend the basic model of Lavoie to different engines and operating conditions [23]. Using the unmixed model of the products and again, assuming negligible heat transfer, NO emissions are calculated for lean, stoichiometric and rich mixtures. These calculations compare well with data taken from experiments over a range of equivalence ratios. The effects of various operating parameters on NO emissions are calculated, including burn duration, timing, EGR%, inlet temperature and pressure, speed, compression ratio, and geometry.

Aiman published experimental results of NO formation and destruction rates emphasizing the importance of these processes in modeling efforts [4]. He stresses the importance of formation kinetics in lean mixtures, because of lower temperatures, and that of decomposition kinetics in stoichiometric mixtures, which have no difficulty reaching equilibrium during the combustion phase. He argues that the absence of heat transfer and mixing in the unmixed model will prevent very accurate results but emphasizes that the usefulness of the models is in showing and explaining qualitative trends.

Heywood and Watts added further detail to their previous model by differentiating among the products in a thermal boundary layer and those in an adiabatic core [6]. The boundary layer is used to transfer heat to the cylinder while the core is isolated and homogeneous as opposed to the unmixed models. Using harmonic functions for the input burn rates, the relations between numerous operating conditions, design parameters and emissions are calculated.

Most recently the question of unmixed modeling of the product region was revisited by Raine, et al [1]. Here, based on the thermodynamic formulations of Ferguson [24] they constructed an unmixed model and showed the effects the number of distinct product regions has on the NO predictions. They conclude that the number of burned zones does have some effect on the NO predictions and that a reasonable number of zones should be on the order of 5 to 10. Raine, et al, also calculates that methane is a good approximation for most natural gas given that the stoichiometric air fuel ratios are adjusted accordingly.

CO has received less attention when compared with the amount of work addressing NO emissions. Newhall's kinetic study, mentioned earlier showed that CO oxidation quenches as temperatures fall

during expansion. [3]. A more detailed study of this quenching in the bulk flow by exhaust valve opening was performed by Delichatsios. Here, portions of the bulk gases were modeled during the late expansion and exhaust phases, showing that the drop in pressures and temperatures quench the CO oxidation process leaving much higher than equilibrium values in the exhaust. Keck and Gillepie also did a kinetic analysis of the important quenching reactions. [8]. Heywood mentions work done by El-Mawla [10] in measuring in-cylinder CO concentrations [22]. Its is found that the quench layer is a major sources of CO and may contribute substantially to CO in lean burn engines.

The most important conclusions to be taken from the previous modeling work are:

1)The NO mechanism should include the Zeldovich reaction with the addition of the OH reaction of Lavioe, et al. (extended Zeldovich mechanism)

2) Temperature and concentration gradients should be modeled in an unmixed or 'semi' mixed fashion.

3) NO formation in the flame zone is unimportant and can be disregarded.

4) Heat transfer may play a role in matching accurately experimental pressure history.

5) The products of combustion in the C-H-O system can be modeled as being in equilibrium at the temperature and pressure of that product element.

6) Methane is a good approximation of natural gas.

2.3 COOK Formulation

The start of burn (SOB), which occurs some time after the ignition angle, marks the beginning of the model's calculations, which are divided into time steps equal to one crank angle, for convenience. Figure 2.1 shows the combustion and cooking cycles, both beginning at SOB, in the context of the engine's entire cycle. The COOK model first calculates the initial conditions based on the isentropic compression of the bottom dead center (BDC) conditions. COOK then proceeds with burning and compressing the mixture. Figure 2.2 shows the overall flow of computations for each time step. Each of the computations will be formulated in more detail in the following sections. Here, Δ is used for all computations made on a crank angle scale and d is used as the

differential time for the integration of the chemical kinetics, a smaller time scale. All thermodynamic and kinetic data needed is calculated in situ using the Chemkin family of subroutines.

2.3.1 Burn Mass Fraction Δm: Determining the Initial Product State

During the engine's combustion phase, a turbulent and scattered reaction zone expands across the volume of the cylinder as it engulfs the reactant mixture. The model interprets this burning phenomena purely through the inputted mass burn rate. Figure 2.3 shows how the sum of the various small differential masses, Δm, which are engulfed in the reaction zones in any one time step during the combustion phase, are represented by the Δm from the burn rate input for that time step. Figure 2.4 shows how that Δm is represented in a typical burn rate curve. At the beginning of the each time step during the combustion phase, one new reactant mass element (Δm) is combusted.

In this model, we are concerned with the fate of certain species as they react as products. As each element of the reactant mixture reacts to become product, it makes a specific transition which needs to be modeled in order for us to begin with an accurate state for the new product element. A simple approximation to burning is the equilibrium state of the reactants. The equilibrium composition and temperature of each new Δm assumes a constant pressure and adiabatic reaction, at the pressure of that crank angle. This resultant composition and temperature becomes the new elements' state and the starting point for its career as a product. The question of the accuracy of this model will addressed during the CO modeling discussion.

The calculation is made using the EQUIL code interface for the Stanjan equilibrium solver. At the beginning of each time step, the mass to be combusted is converted to its equilibrium state and returned. This conversion releases energy which is stored by the code as the $\Delta U_{combustion}$ (ΔU_c) for this time step. This heat release will be used in the energy equation at the end of the time step to update the cylinder pressure. The equilibrium calculation transforms the reactant mixture of fuel and air, whatever that may be, to a mixture of products, again, whatever is decided to be of importance to the particular fuel or operating conditions present. This is where COOK is different from previous engine models. There, the subroutines for calculating the kinetics were fixed by those kinetics, written based on the equilibrium and steady state assumptions used in the kinetic

calculations. COOK is built around an input chemical mechanism which enables total flexibility of type of fuel, oxidizer, atmospheric conditions, and level of detail. Simply by changing the chemical mechanism file, a new fuel or products of combustion can be used in the model where the only limitation is computer memory and speed.

The products of combustion used in the transition calculation depend upon the mechanism used in the model. COOK's flexibility arises here where the only limits on the type of fuel, oxidizer , or diluent used are whether or not thermodynamic and kinetic data are available for all of the pertinent species.

A multizone model assumes that the products are divided into several distinct segments which are isolated chemically and thermally. Raine, et al [1] concluded that between 5 and 10 is an optimal number of segments, balancing computational practicality and realistic level of product interaction. Burn durations are sometimes over 70 crank angles and for each crank angle there is a separate Δm. COOK combines consecutive Δms into product segments as they are converted to products. That is, if there are 70 Δms to be combined to make 10 product segments, each set of 7 consecutive Δms are merged together into a product segment as they emerge from the burn calculation.

2.3.2 Product Segments React: Cooking

Each product segment, whether it is filled or still receiving new Δms, undergoes the cooking calculations. Here, kinetic calculations are carried out on each product segment as it is further compressed or expanded by both the piston motion and the combustion and reactions of new Δms. Each product segment is treated separately as a plug flow and its reactions are carried out under the constant pressure of that time step. Here, the code was adapted from the Senkin code for constant pressure, adiabatic, plug flow calculations. Again, all of the kinetic and thermodynamic data are supplied by the Chemkin subroutines.

The formation (or destruction) of each species k results from the elementary reactions, i, in which they participate:

$$\frac{dY_k}{dt} = v\dot{\omega}_k W_k \qquad (2.1)$$

where $$\dot{\omega}_k = \sum_{i=1}^{I} \nu_{ki} q_i \tag{2.2}$$

and $$\nu_{ki} = \left(\nu''_{ki} - \nu'_{ki}\right) \tag{2.3}$$

and $$q_i = k_{fi} \prod_{k=1}^{K} [X_k]^{n'_{ki}} - k_{bi} \prod_{k=1}^{K} [X_k]^{n''_{ki}}. \tag{2.4}$$

Y_k is the mass fraction, $\dot{\omega}_k$ is the molar production rate, W_k is the molar mass, all for species k, and v is the specific volume, q_i is the rate of progress for the reaction i and the V_{ki}s are the stoichiometric coefficients for species k for reaction i. X_k is the molar fraction of species k and K_{fi} and K_{bi} are the forward and reverse reaction rates for the elementary reaction, *i*. Each elementary reaction obeys the law of mass action and its rate is given by the Arrhenius relation:

$$k_{fi} = A_i T^{B_i} \exp\left(\frac{-E_i}{R_c T}\right) \tag{2.5}$$

where B_i, the temperature exponent, A_i , the pre-expontial factor, and E_i, the activation energy, are specified in the chemical kinetics mechanism (see section 2.41). For each segment, mass is conserved:

$$\frac{dm}{dt} = 0 \tag{2.6}$$

along with energy at constant pressure, adiabatic

$$de + pdv = 0. \tag{2.7}$$

Substituting h, the specific enthalpy, for e gives us dh = 0 and

$$h = \sum_{k=1}^{K} Y_k h_k \tag{2.8}$$

so,
$$dh = C_p\frac{dT}{dt} + \sum_{k=1}^{K} dY_k h_k \tag{2.9}$$

$$= C_p\frac{dT}{dt} + v\sum_{k=1}^{K} h_k\dot{\omega}_k W_k = 0. \tag{2.10}$$

where C_p is the constant pressure specific heat. Equations 2.10 and 2.1 (for each species) are then integrated over the duration of one time step,

$$\Delta t = \Delta\theta/\omega$$

where $\Delta\theta$ is one crank angle increment and ω is the engine's rotational speed.

Thus, for each product segment, the array of species is reacted through one time step. The heat released (or absorbed) by these reactions is stored as the $\Delta U_{reaction}$ (ΔU_r) and as the code cycles through each separate segment, these ΔU_rs are summed.

2.3.3 Pressure Calculation

The two energy releases, ΔU_c and ΔU_r, heat transfer, ΔQ, and the work transfer, ΔW, from the movement of the piston contribute to the changing pressure inside the cylinder. The pressure is considered to be spatially uniform since the time needed for pressure waves to equilibrate spatial pressure gradients is much smaller than one crank angle. The pressure, P, unburned temperature, T_u, and the average product temperature, T_b, are calculated at the end of each crank angle using the first and second law and the conservation of volume, v, and mass, m:

$$V = v_u m_u + v_b m_b \tag{2.11}$$

$$m_{total} = m_u + m_b \tag{2.12}$$

$$\Delta U_s = \Delta W + \Delta Q_{ch} - \Delta Q_{ht} \tag{2.13}$$

where $\Delta W = -PdV$ (2.14)

$\Delta U_s = m_u C_{vu} \Delta T_u + m_b C_{vb} \Delta T_b$ (change in sensible energy), (2.15)

$\Delta Q_{ch} = \Delta U_c + \Delta U_r$ (change in chemical energy) (2.16)

ΔQ_{ht} = heat transfer (2.17)

and v is the specifc volume.

Note that C_{vb} is the mass averaged C_v for all the burned segments. The ΔT are each evaluated by the second law for the unburned and burnt masses where 1 denotes the beginning and 2 denotes the end of the crank angle and i denotes either burnt or unburnt.

$$\Delta T_i = T_{2i} - T_{1i}$$

$$= T_{1i}\left(\frac{P_2}{P_1}^{\frac{\gamma - 1}{\gamma}} - 1\right) \qquad \text{where } \gamma \text{ is the ratio of the specific heats.} \tag{2.18}$$

Values like T_b, C_{vb}:, and γ are the mass weighted average quantities for all the product segments, such as:

$$T_b = \frac{1}{M_b}\sum_{i=1}^{I} m_{bi} T_i \tag{2.19}$$

where m_{bi} are the product segments' masses and M_b is the total burned mass.

Substituting 2.18 into 2.15, and 2.14, 2.15, 2.16 and 2.17 into 2.13 leaves an equation in P. Combining Eq 2.11 with Eqs 2.12 and 2.13 and iterating will give the Ts and P for the end of the

crank angle.

The exhaust CO and NO calculations are made by a mass weighted average of the segments' concentrations at a point sufficiently late in the expansion phase to allow the important reactions to freeze. This is typically at around 110 to 140 degrees ATDC. The level of CO and NO at this point in the cycle should reflect well the exhaust concentrations since the temperatures in the exhaust are too low to affect the major C-H-O and N-O reactions. Typical exhaust gas temperatures in the manifold are below 900°K.

2.3.4 Initial Conditions

The model begins calculation of the post flame reactions at the SOB. Needed at this point are the thermodynamic conditions of the reactant mixture. These are found by isentropically compressing the fuel and air mixture from the BDC conditions.

The isentropic compression of the mixture assumes constant C_v and C_p over the range of compression temperatures, taken at a temperature, T_{ave} roughly in between that of the BDC (the zero state, i.e. Vo) and SOB:

$$\gamma = C_p / C_v \quad \text{where } T_{ave} = (T_{in} + 800)/2 \tag{2.20}$$

and

$$\frac{T_{SOB}}{T_o} = \left(\frac{V_o}{V_{SOB}}\right)^{\gamma - 1} \tag{2.21}$$

and

$$\frac{P_{SOB}}{P_o} = \left(\frac{V_o}{V_{SOB}}\right)^{\gamma}. \tag{2.22}$$

Note that in the cases where the fuel to air equivalence ratio, ϕ, is distributed around the average, as during part of the CO study, the compression to SOB calculation is done on a mixture of exactly the average air fuel ratio.

2.4 Inputs

COOK's array of input enables it to be tailored to many different operating configurations. A list of

the most important inputs includes (some of which will be discussed in more detail in the following sections):

1. Air to fuel equivalence ratio, Lambda, λ ($1/\phi$)
2. Angle of Start of Burn
3. Angle of End of Burn
4. Level of unmixidness (see section 4.4)
5. # of crank angles per product segment
6. Separate chemical mechanisms for burning and cooking
7. Compression ratio
8. Heat transfer fraction
9. % Exhaust gas recycled
10. Engine Speed
11. Stoichiometric (volumetric) air fuel ratio
12. Ending crank angle
13. BDC pressure
14. BDC temperature

2.4.1 Chemistry

The chemical aspects of COOK was discussed briefly in section 2.31 concerning the transition from reactant to product. Since the mechanism used in COOK is an input, the chemical capabilities of the model are enormous. Various mechanisms have been developed for the combustion of various fuels having different levels of detail, including multiple phases, soot and other phenomena which Chemkin and its libraries are capable of handling. Since COOK is written on the Chemkin platform, it can be used in conjunction with any of Chemkin's capabilities. For this discussion, however, the focus is on the NO and CO chemistry of methane combustion.

An important input to the model are the chemical properties of the reactants and products. These come in the form of a set of thermodynamic and rate data for all species and relevant elementary reactions for the fuel and oxidizer in question. The engines to be modeled operate on a mixture of air and natural gas. The composition of natural gas varies and a typical composition might look like:

Volume Fraction (%)	Constituent

94.15	Methane
3.00	Ethane
0.53	Propane
0.09	i-Butane
0.10	n-Butane
0.06	C5+
0.73	Carbon Dioxide
1.34	Nitrogen

Raine, et al [1] verifies that methane is a very good approximation to natural gas for the type of calculations being made here. The fuel used in the model consisted of:

Volume Fraction (%)	Constituent
98.6	Methane
1.4	Nitrogen.

The input fuel-air mixture is calculated as:

$$\phi \text{ Fuel} + [\lambda_s(O_2 + 3.76N_2)]/4.76 \qquad (2.23)$$

where ϕ = equivalence ratio

λ_s = stoichiometric (volumetric) air fuel ratio, (9.5 for CH_4) .

EGR, a mixture of H_2O, CO_2, N2 and O_2, is then added as a volume percentage of the total air-fuel mixture. The EGR composition depends upon the fuel air ratio being modeled.

The thermodynamic properties of all species relevant to the combustion of methane are needed and supplied by a thermodynamic database. It consists of a listing of polynomial coefficients for C_p, H_o, and S_o over several connected temperature ranges. This data base is then read by the Chemkin interpreter code for use in gathering data during the computation.

The mechanism is a very important input to the model from both the standpoint of accuracy and complexity. Each reversible elementary reaction requires a separate pair of rates to be integrated. Choosing the most important reactions is very important so as to minimize needless computational effort. The most advanced reaction set for methane combustion is the GRI-mech, which has over 200 reactions for 34 species. The computational time, however, required to run the model using this set is substantial. A reduced methane mechanism, Methmech, was found and compared to the

results for GRI-mech. Figure 2.5 shows the concentration histories of a few species during a typical run. The Methmech reaction set was used in all of the runs in this work and is listed in appendix A.

The effects of having a mechanism without the higher carbon species of true natural gas (propane, ethane, etc.) are probably small for the type of model this is. Since all combustion which occurs is considered complete under the equilibrium transition model, the higher carbon species would not be significant among the product reactions, since the volumetric fraction of the higher carbons in the reactants is rarely more that a few percent. Blumberg briefly outlines typical NO emissions from different fueled engines:

Fuel	NO (ppm)
Methane	1200
Propane	1800

Taking this difference into account and the fractions of higher carbons like propane in natural gas, the error incurred would be less than 2 percent. The effects on carbon monoxide might be higher but compared to other sources of error in the model, it is again, insignificant.

The NO formation mechanism is based on those used in earlier work, namely, the extended Zeldovich mechanism. These rates are found in [34] which are quoted in [33,p168].

$N_2 + O \leftrightarrow NO + N$ $\quad k_f = 1.8E14 \exp(-76{,}241/RT)$

$\quad k_b = 3.8E13 \exp(-844/RT)$

$N + O_2 \leftrightarrow NO + O$ $\quad k_f = 1.8E10\ T \exp(-9299/RT)$

$\quad k_b = 3.8E9\ T \exp(-41{,}369/RT)$

$N + OH \leftrightarrow NO + H$ $\quad k_f = 7.1E13 \exp(-894/RT)$

$\quad k_b = 1.7E14 \exp(-48{,}800/RT)$

The primary CO oxidation reactions are:

$CO + O + M \leftrightarrow CO_2 + M$ $\quad k_f = 3.2E13 \exp(4200/RT)$

$CO + OH <--> CO_2 + H$ $k_f = 1.51E7\ T^{1.3} \exp(758/RT)$

$CO + O_2 <--> CO_2 + O$ $k_f = 1.6E13 \exp(-41{,}000/RT)$

2.4.2 Burn Rate

The simplicity of this model in computing the thermochemistry of the products results from its ignorance of the fluid mechanics and flame propagation. The main importance of the fluid mechanical and combustion calculations to the post flame reactions is the resultant burn rate. This rate dictates to a zero dimensional model like COOK the rate of product formation. The burn rate is influenced by changes in geometry, spark plug location, timing, turbulence, mixing, and other effects of operating parameters and engine designs.

The burn rate is input from either experimental measurements or computed as an exponential function approximating common burn rate shapes. The experimental burn rates are computed from the pressure measurements made on the engines being simulated at the conditions to be modeled and typically look like figure 2.6. The form of exponential functions which approximate this turbulent burning history was first introduced by Weibe and look like:

$$X = 1 = \exp(-a(\theta - \theta_o)/\Delta\theta)^{(m+1)} \qquad (2.24)$$

where X is the fraction of total charge burnt as of crank angle θ

a and m are shape factors

θ_o is the angle of start of burn

$\Delta\theta$ is the burn duration.

Figure 2.7 shows the effects a and m have on the shape of the burn rate.

2.4.3 Heat Transfer

Heat transfer is a known function input to the model. Here, the level of heat transfer is specified as a fraction of the chemical energy deposited in the cylinder by the charge. The fraction of heat

transfer since the shape of the energy deposition history is similar to the shape of the heat transfer deposition history. This fraction is typically on the order of one percent.

$$Ht(\theta) = A + B(\theta) \tag{2.25}$$

$$\Delta Q_{ht} = Ht\, \Delta Q_{ch} \tag{2.26}$$

2.4.4 BDC Conditions

The post flame calculations central to this model begin at the start of burn. To calculate the conditions of the mixture at that point, the BDC conditions must be given. These include:

1. inlet temperature, T_o , which is calculated as roughly a mass weighted mixture of residual burnt gases at high temperature and inlet gases at ambient temperature. This temperature differs for lean and rich mixtures since the residual gases' temperatures vary with equivalence ratio.

$$T_o = T_{in}X_{in} + T_{res}X_{res} \tag{2.27}$$

where T_{in} = temperature of inlet gases (ambient)

X_{in} = mass fraction of inlet gases in cylinder at BDC

T_{res} = temperature of residual gases

X_{res} = mass fraction of residual gases in cylinder at BDC.

2. BDC pressure, P_o which is taken approximately from the experimental data when the model is being used to approximate an experiment, or 1 atmosphere in other cases.

2.4.5 Geometry

As the engine's crank shaft turns and the piston fall and rises, the volume of the system being modeled changes. Figure 2.8 shows the geometric relations among moving parts. The changing volume is specified as a function of crank angle based on the piston rod length, 1, crank arm length, a, clearance volume V_c:

$$V(\theta) = V_c + A\,(l + a - s) \tag{2.28}$$

where $s = a\cos\theta + (l^2 - a^2\sin^2\theta)^{1/2}$

A = cylinder cross section area = $\pi B^2/4$

B = cylinder bore

$r_c = V_{max}/V_c$.

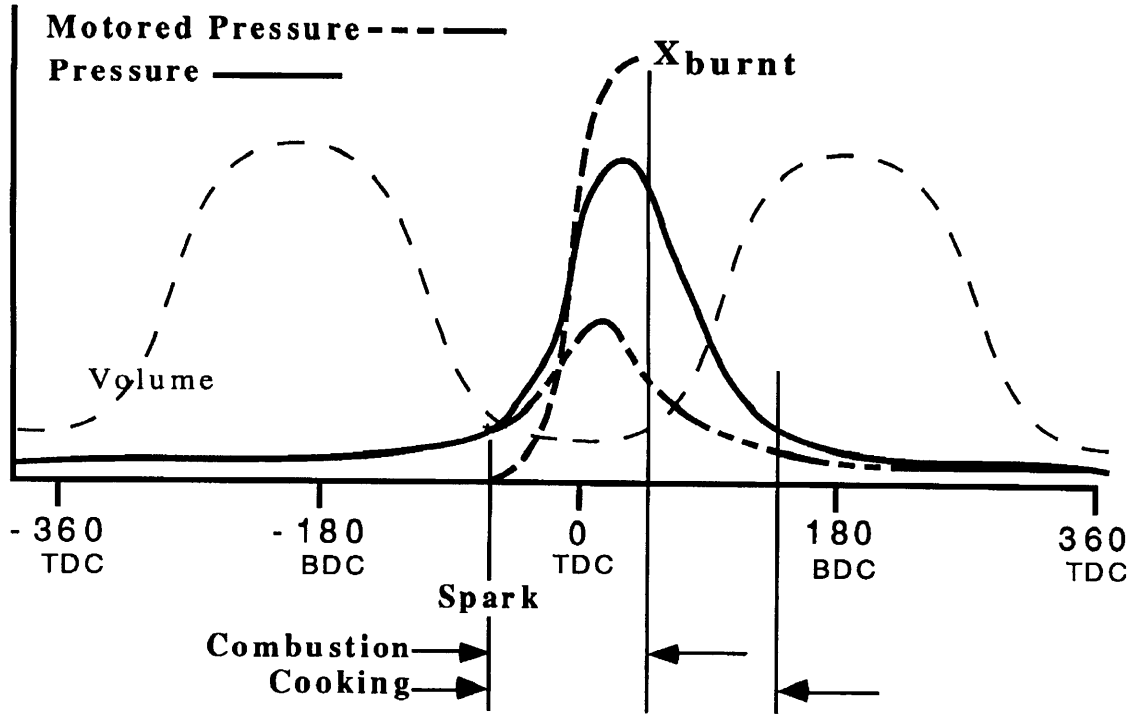

Figure 2.1 COOK model regime of operation includes the combustion and cooking phases.

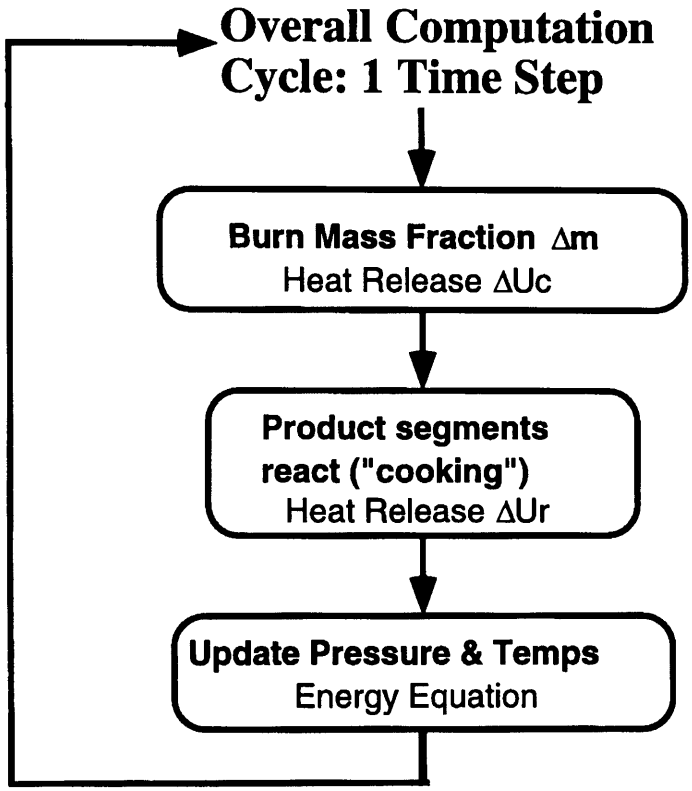

Figure 2.2 Overall computational cycle in COOK model.

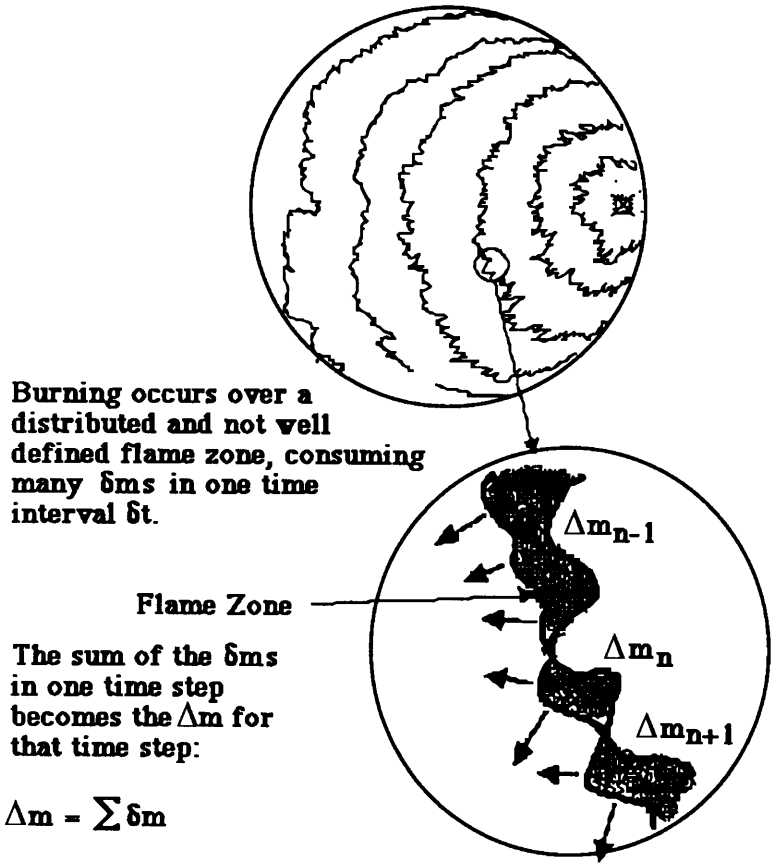

Figure 2.3 Physical representation of Δm used in burn rate.

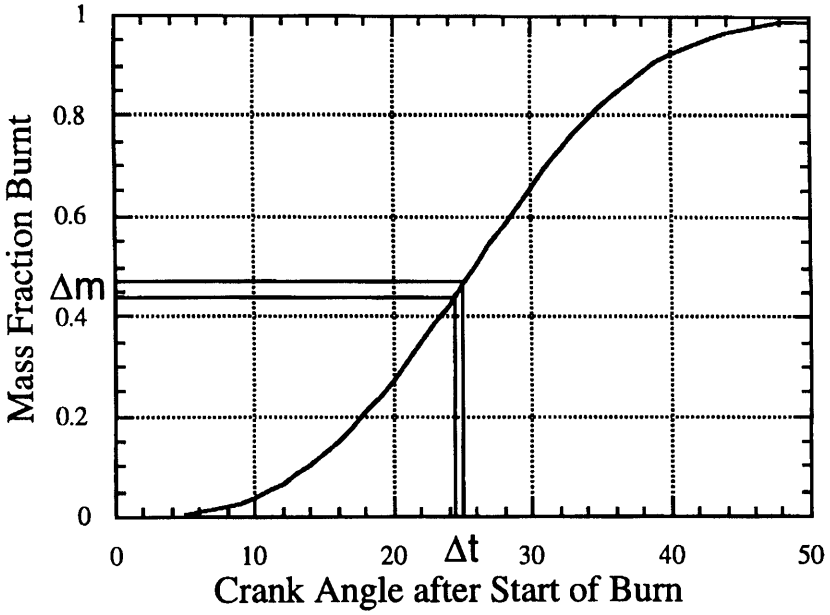

Figure 2.4 Δm as it is represented in a typical mass fraction profile input.

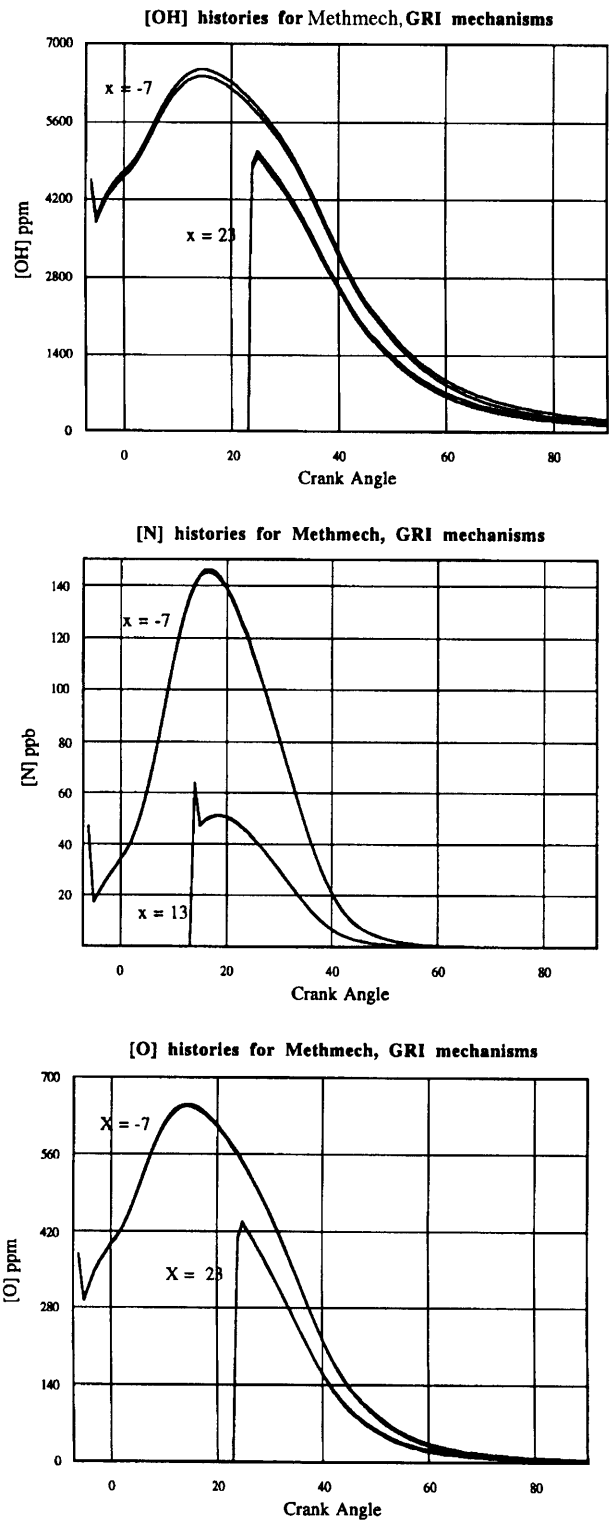

Figure 2.5 Comparisons of several species' concentration histories using both GRImech and Methmech showing their very strong agreement (much of the histories are indistinguishable). The Xs denote at what crank angle the mass element plotted was initially burned.

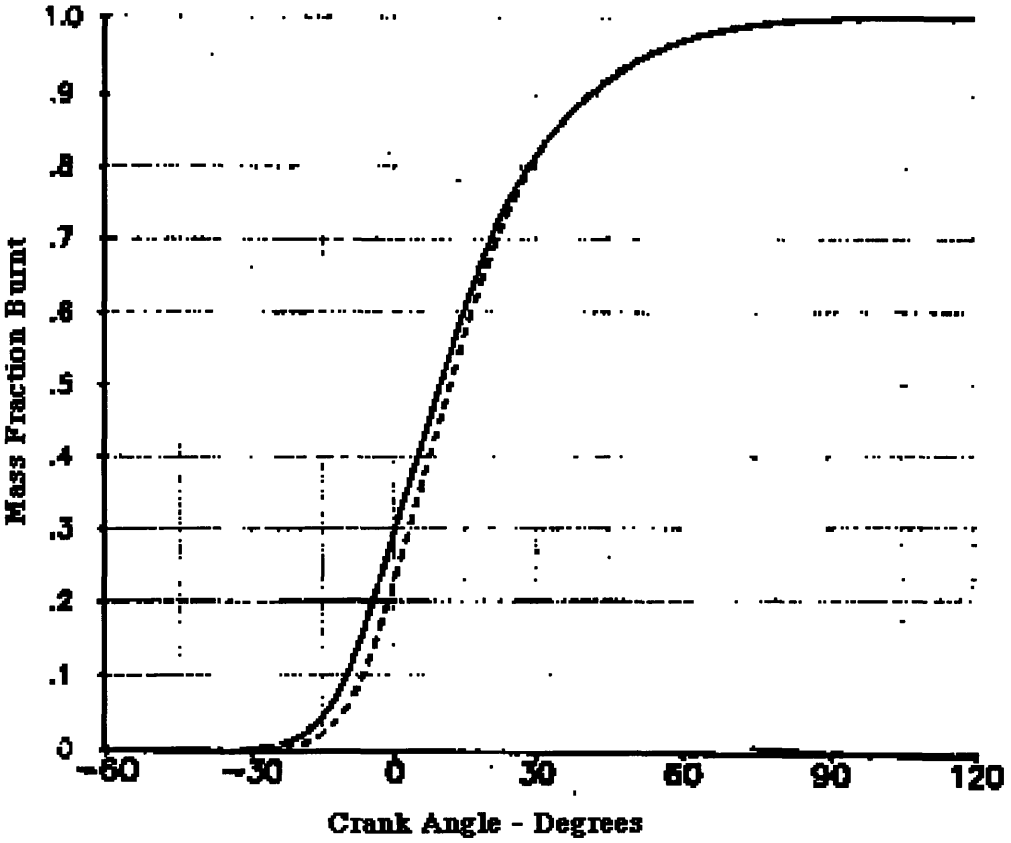

Figure 2.6 Typical input burn rate from experiment showing data from 2 similar runs.

W

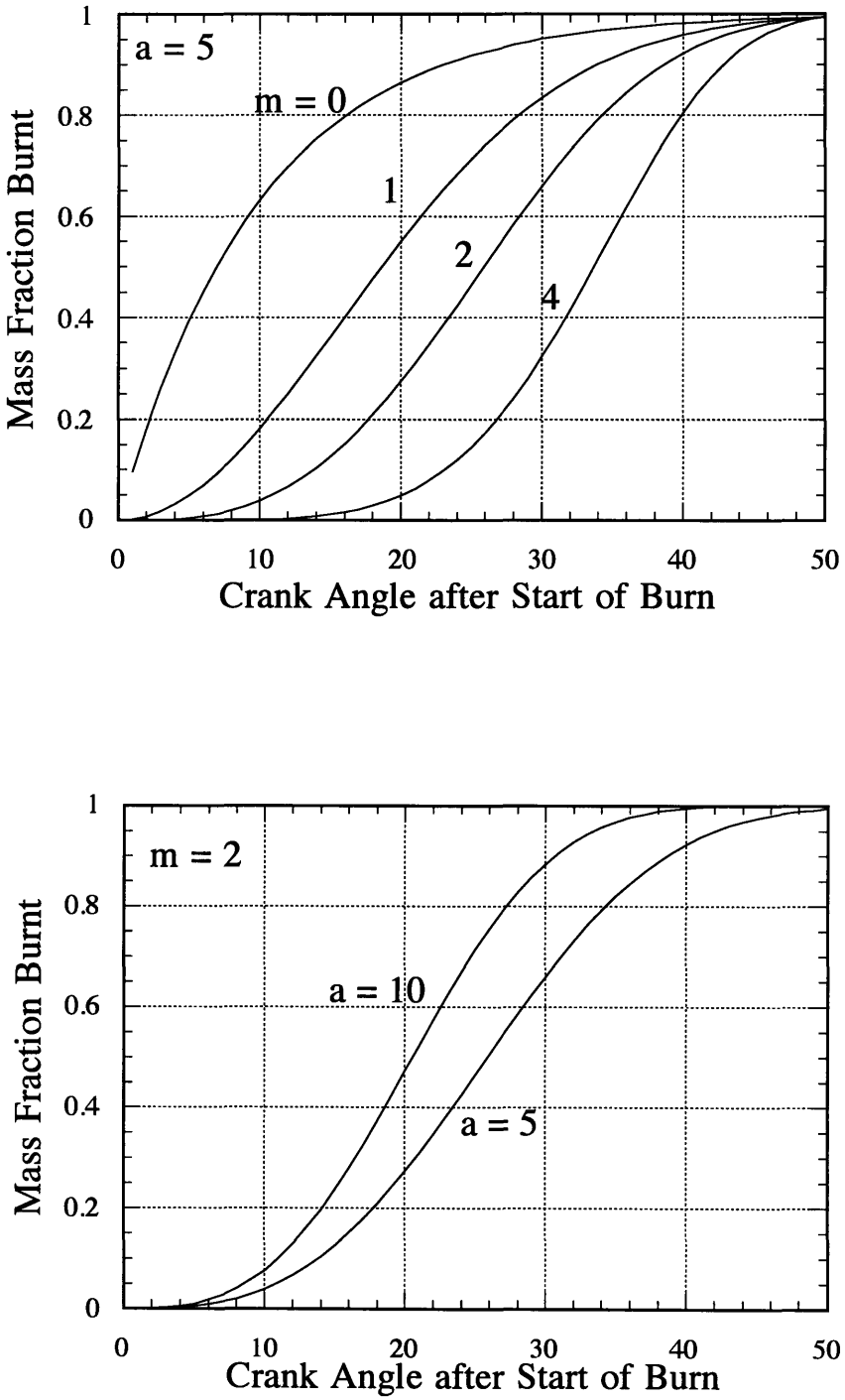

Figure 2.7 Weibe functions with varying a and m shape parameters.

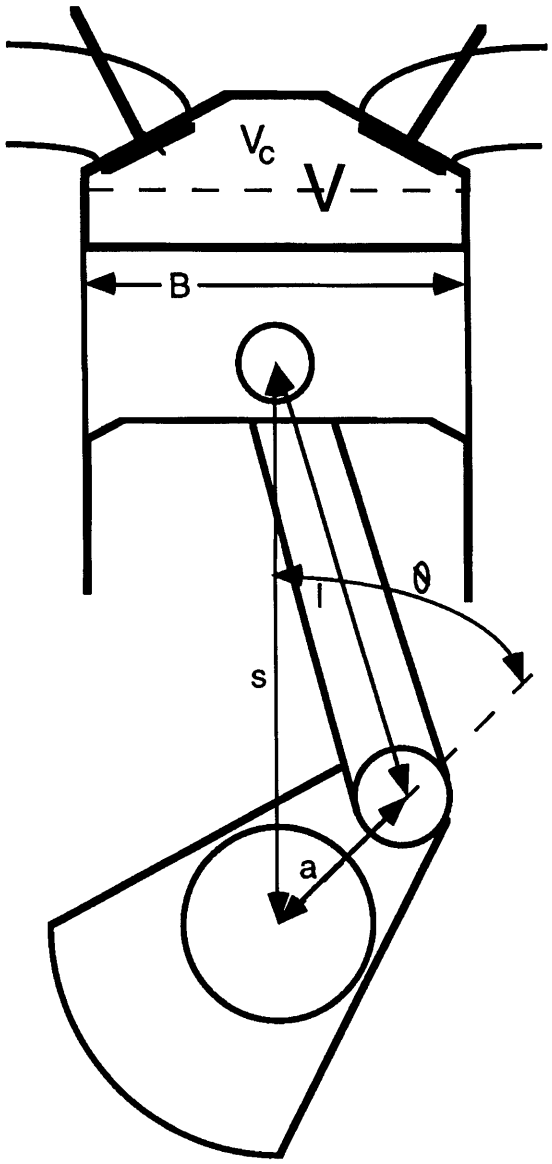

Figure 2.8 Engine's crank and piston geometry.

3. NO Emissions Modeling

3.1 Introduction

The COOK model was used to predict NO emissions and to help better understand the mechanisms behind NO formation in lean, natural gas engines. This chapter will outline the results of the NO studies, beginning with comparisons with experimental data and earlier qualitative work in NO emissions modeling. These comparisons help to highlight the important mechanisms for NO formation in lean engines. Some discussion will follow concerning NO reduction strategies.

Before preceding with the NO modeling, it should be noted that the level of product segmentation used in the COOK model can have an effect on the NO results. Figure 3.1 shows that keeping a more segmented product region lowers NO predictions, which is in agreement with earlier researchers [1]. This variation in NO is only a few percent over the range of numbers used in this study. Most of the study was done with over 10 and as many as 100 product segments.

The NO predictions are very sensitive to inputs like pressure and temperature and there are corresponding errors associated with these inputs. Since they are important to the behavior of the model, they will be discussed in more detail later. Using COOK to predict experimental results taking inputs from experimental data means there are some errors in the predictions based solely on errors in the inputs. These errors will not be quantified here, but were estimated to be around 5 to 7 percent based on the sensitivity of COOK to its inputs.

During this work, COOK was used to predict both experimental data as well as to illustrate trends and verify other known phenomena. When used to approximate experimental conditions, COOK is used with burn rate inputs which are digitized from the experimental data. Data in this form look like that shown in figure 2.6. In doing more qualitative work, a standard Wiebe function burn rate is used with shape parameters a set to 5 and m set to 2. This burn rate shape is used for all of the different burn durations. Generally above each plot, the speed, phi or case number for the experiment will be labeled. Where burn durations are not specified, 50 degrees is used. This is the

case when comparing different engine speeds, ignition timing and mixture equivalence ratios. While using a constant burn rate under all of these conditions is not rigorous, for doing qualitative studies, it is not unreasonable. Qualitative work is used to establish trends and rarely to make definitive comparisons. In plotting the NO versus phi in figure 3.7, certainly the burn rates are faster near stoichiometric, but this would not affect much the main aim of the plot, which is to compare the location of the peak with that of the experimental data. For trends where speed is varied, a constant crank angle burn rate is fairly accurate, considering that turbulence levels scale with piston speed making higher speeds have correspondingly faster burn rates. Past researchers doing qualitative work have as well used fixed burn rates.

3.2 Experimental Comparisons

Comparisons with experimental data show how well COOK predicts NO over a range of operating conditions. The experimental data was taken from progress reports during development work for a production natural gas engine. The specifications for this engine are:

single cylinder, 4 stroke, Carbureted

Swept volume	272.6 cc
Bore:	73.03 mm
Stroke:	65.08 mm
Compression Ratio	12.80:1
L/a	1.71942

Different heads and intake systems were used in several of the tests but these are related to COOK solely via the burn rate data taken from the experiment. The case numbers and their conditions will be presented in tabular form, followed by the NO measurements and the COOK predictions. All future references to cases by number are referring to these listed cases.

Table 3.1 Experimental Cases.

Case #	Phi	Speed (rpm)	Spark Timing (°ATDC)	SOB (°ATDC)
1	0.91	3600	-15	-6
2	0.91	3600	-25	-15
3	0.91	3600	-35	-25
4	0.67	3000	-55	-33
5	0.67	3000	-40	-21
6	0.68	3000	-50	-26
7	0.65	3000	-40	-24
8	0.65	3000	-20	-9
9	0.63	3000	-50	-23

Table 3.2 NO comparisons

Case#	NO emissions (measured ppm)	NO emissions (predicted ppm)	%Difference
1	1735	1716	1.1
2	3115	3210	3.0
3	3832	3996	4.3
4	462	352	23.8
5	276	254	8.0
6	242	145	40.8
7	948	873	7.9
8	93	67	28.0
9	149	89	40.3

Graphically, figure 3.2 shows COOK's relatively good agreement with the trends of the experimental data. The pressure traces in figures 3.3 and 3.4 also show for three of the cases how well the pressure cycle was simulated. The differences between the predictions and measurements, however, point out that prediction for the leaner cases is more difficult than the richer (#1-3) cases. The differences in prediction accuracy between the 0.91 fuel/air ratio and the 0.66 fuel/air ratio point to a fundamental difference in the way NO forms under the two conditions.

3.3 NO Formation Issues

NO is formed via the extended Zeldovich mechanism [33, p168]:

$N_2 + O <--> NO + N$ $\quad k_f = 1.8E14 \exp(-76{,}241/RT)$

$\quad k_b = 3.8E13 \exp(-844/RT)$

$N + O_2 <--> NO + O$ $\quad k_f = 1.8E10\ T \exp(-9299/RT)$

$\quad k_b = 3.8E9\ T \exp(-41{,}369/RT)$

$N + OH <--> NO + H$ $\quad k_f = 7.1E13 \exp(-894/RT)$

$\quad k_b = 1.7E14 \exp(-48{,}800/RT)$

which, due to its high activation energies, makes NO formation a high temperature phenomenon. The integration of these rates at different temperatures in Figure 3.5 shows the dependence of the NO formation kinetics on temperature. These natural gas engines easily achieve temperatures

which facilitate NO formation, but the limiting factor once these temperatures are reached is time.

Each product segment goes through a distinct temperature and pressure history, yielding its distinct chemical makeup at the point of exhaust. Some product segments attain the NO kinetic threshold of 2000°K only for a short time. Others, typically those which burn first and undergo compression, spend a longer time at high temperatures. Figure 3.6 shows how NO tends to be concentrated in the first few elements burned.

All chemical processes asymptotically move towards equilibrium at a finite rate. The temperature dependent kinetics of NO formation/decomposition determine how fast the NO reactions occur, and its equilibrium concentration with respect to its current concentration determine whether it is being formed or destroyed. As a product segment is compressed, its NO equilibrium value rises, and if the NO kinetics are fast enough, the actual NO level will 'keep up' with its equilibrium. After a certain point during expansion, the temperature of the element is dropping which slows the kinetics and lowers the equilibrium concentration. Below around 2000°K, the kinetics can no longer keep up with the speed of the falling equilibrium levels and the NO reactions become frozen. The NO concentration levels off above the descending equilibrium values. This equilibrium 'chasing' is key to understanding the different sensitivities and issues in modeling NO emissions.

NO for different fuel to air ratios is shown in figure 3.7, along with some other published data for a different engine and fuel. Here, the equivalence ratios which produce the maximum NO match fairly well with the peak of the data presented in [23] by Robison. Robison's models were for a gasoline engine at 1500 rpm and a compression ratio of about 8.5. This peak matches other published plots as well and is evidence of the general accuracy of the COOK model. The location of the peak is affected by both the kinetics of the NO formation and destruction but as well the equilibrium values, both of which demand accurate calculation of the thermodynamic histories of the product segments. This peak sits just at the point between where the O concentration becomes high and temperatures become high. High temperatures affect speed, while the O concentration, which grows as the fuel air ratio drops, affects the NO equilibrium. While NO equilibrium peaks at around $\phi = 0.75$ and drops off on both sides, temperatures peak at about $\phi = 1.08$ and drops off on both sides as well. Where the two phenomena act in conjunction, that is where speeds are high enough to reach equilibrium and that equilibrium concentration is high, is within the region between the two peaks, or, roughly $\phi = 0.9$. This is shown clearly in the data of Robison as well as from the COOK predictions.

3.3.1 NO Formation at Rich Conditions

Both the stoichiometric and rich cases achieve temperatures which allow NO to approach equilibrium and then decompose during expansion. Because of the low O_2 concentration under rich conditions, NO equilibrium values are very low and while the temperatures are also fairly low, they yield NO formation rates fast enough to allow NO to follow its equilibrium fairly closely. Figure 3.8 and 3.9 show the temperature histories for several product elements as well as their corresponding NO histories. Here, NO values eventually level off as the temperatures drop below the 2000°K threshold.

3.3.2 NO Formation at Stoichiometric conditions

The stoichiometric region yields the highest temperatures and the highest NO emissions, as is shown in figure 3.7. Figures 3.10 and 3.11 show the temperature and NO histories for the first, middle and last burned elements for the $\phi = 1.0$ case.

The first product segments burned achieve very high temperatures after the energy of the rest of the charge is released, compressing the mixture along with the piston motion. Here, NO equilibrium values are high, and the kinetics are fast enough to reach those values. As the piston falls along with the temperatures, so do the NO equilibrium values for the first burned elements. The kinetics follow the equilibrium for some time until the rates are too slow and NO decomposition in these elements become frozen. NO levels in the later burned elements are constrained by the kinetics to even reach their equilibrium level by the time they become frozen. These later burned elements are formation limited.

3.3.3 NO Formation at Lean conditions

Comparing the COOK predictions to the experimental data illustrates that there is more difficulty in predicting emissions for the leaner cases ($\phi = 0.66$) than for the near stoichiometric ($\phi = 0.91$) cases. The lean cases are more sensitive to changes in the engine parameters and time scales which makes modeling lean engines more difficult and prone to error. Comparisons with the stoichiometric case will illustrate these mechanisms more easily.

Figures 3.12 and 3.13 show the temperature and NO histories for several product segments in a

typical lean model. While the NO equilibrium values are extremely high (notice that they are higher than the stoichiometric case), the temperatures and reaction rates are low. This slows NO formation and does not allow it to reach its equilibrium values. The NO is formation limited and its exhaust levels are determined solely by its formation. This means that when formation time scales lengthen, either by slowing engine speed, or by increasing the reaction kinetics via temperature, more NO is formed, and likewise when they shorten, less NO forms.

In a stoichiometric engine, on the other hand, NO emissions are much less sensitive to changes in time scales. As they lengthen, more NO forms in the later, formation limited region but more NO burns out in the early burning, decomposition limited product region. Thus, the competing forming and decomposing processes make NO prediction in richer engines much more stable and accurate.

Figure 3.14 illustrates the different responses a lean and a stoichiometric engine have to changing engine speed. All of these runs were done with a Wiebe function burn rate and a burn duration of 50 degrees. For illustration, figures 3.15 and 3.16 show the different temperature histories for different engine speeds, 3500 and 5500 rpm in a lean engine. The effects of the time scales can be seen in figures 3.17 and 3.18 where both a lean $\phi = 0.66$ and a richer $\phi = 1.0$ case are run over a variety of engine speeds. Notice that in the richer case, the slower engine produces more NO in the later products and less in the earlier, illustrating the balancing of the formation and decomposition. In the lean engine in figure 3.17, the slower engine produces more NO in both the early and later burned elements. Another example of the different NO formation processes can be seen in the effects of rising temperatures via increased maximum pressures (which are effected nearly linearly by the BDC pressure input), as shown in figure 3.19. Again, the formation limited lean engine is much more sensitive to the changing inputs.

This sensitivity makes prediction of NO in lean engines more difficult than in stoichiometric engines. When attempting to input parameters like BDC pressure and temperature from experimental data the sensitivity to these inputs makes accurate prediction tricky. This explains the relative inaccuracy in the predictions for the leaner engine as well as helps to elucidate the dominant NO forming mechanisms in lean engines. Qualitatively, COOK can be used to show trends in NO emissions and efficiency for lean engines.

Numerous engine parameters effect the temperatures and time scales which control NO formation. NO emissions dependence on compression ratio and volume % exhaust gas recycle (egr) are shown in figures 3.20 and 3.21 respectively.

Changing the temperature-pressure history of the charge can also be achieved by burning the charge earlier or over a different duration. Combustion duration is dependent on spark location, turbulence levels within the charge, and is also affected by the spark timing. Brake specific NO (BSNO) emissions are calculated by dividing the mass of NO emitted by the total work energy, E_w, output from the engine:

$$E_w = \sum_{cycle} P\Delta V$$

where P is the pressure and ΔV is the discrete change in volume for the time step. Brake specific fuel consumption (BSFC) is the mass of fuel divided by the work energy output. Typical burn durations of lean gas engines are between 50 and 90 crank angles. Figure 3.22 shows the effects of changing the spark timing and changing the combustion duration on the specific NO emissions. Here, fuel consumption changes as the burn duration is moved and shortened, which is shown in figure 3.23. Trends like this can help in determining the relative importance of different development ideas and operating conditions to optimize.

3.4 Effects of Heat Transfer and Crevices on NO

This work and much of the previous work done in NO prediction have assumed heat transfer was negligible. An accurate formulation of a heat transfer model would be to have a boundary layer at the walls and an adiabatic core of products. This has been implemented successfully in Poulos [37] and others. COOK's energy equation is solved for the bulk gas and no differentiation is made between the boundary layer and the insulated gases. As a result, heat transfer in this model has an unrealistically profound effect on NO predictions, since heat is taken equally from all the product elements. In a more accurate boundary layer model, the NO emissions would be affected very little since the central product elements, or those burned first, contain the most NO (figure 3.6) and would not loose heat to the wall. Transferring heat from all of the gas elements uniformly as in COOK will drastically change NO predictions as is shown in figure 3.24. A loss of only 3% will drop NO predictions by 50%.

No heat transfer was used in any of the runs previously presented. Notice that there is a difference between the effects heat transfer has on a very lean (ϕ =0.66) and a more rich (ϕ =0.91) mixture.

Crevice and wall interaction take place late in the burning event and, as was shown, would change only negligibly the total NO produced in the core burned zone. Crevices could decrease NO by lowering combustion efficiency and thus peak temperatures and by leaving some of the fuel unburned.

3.5 N_2O Pathway Effects

One benefit of COOK's chemical flexibility is that different mechanisms can be tested for their significance in modeling of the engine's emissions. Previous research implicates the N_2O mechanism for the formation of NO in methane combustion systems. Here, N_2O is formed and then decomposes into NO:

$N_2O + O <--> 2NO$ $\qquad k_f = 2.9E13 \exp(-23150/RT)$

or

$N_2O + O <--> N_2 + O_2$ $\qquad k_f = 1.4E13 \exp(-10810/RT)$

Experimental results show that in high temperature stirred reactors, this pathway yields identical results to that of the purely thermal (Zeldovich) mechanism over the lean range of conditions investigated here [39]. Using the GRImech 2.11 with the most up to date and complete set of Nitrogen chemistry including these key N_2O reactions shows that indeed for the lean ranges discussed in this paper, the N_2O mechanism is not significant. Figure 3.25 shows the comparison over the lean range between the standard mechanism, Methmech with the purely thermal NO chemistry and the GRImech 2.11, with the complete nitrogen chemistry.

3.6 Conclusions

A fundamentally based thermochemical model has been constructed to calculate NO concentrations in a very flexible manner, enabling a wide variety of parameters and operating conditions to be modeled. Difficulty in predicting the NO emissions for leaner engines led to a better illustration of the key mechanisms in NO formation. Lean mixtures' sensitivities to time scales and rate changes result from their formation limited processes which are in contrast to the richer mixtures, whose NO emissions are a result of both formation and decomposition processes. Qualitative trends can be produced using COOK to show the effects changing parameters have on engine emissions and

efficiency. Changing mechanisms gives insight into the dependence the NO have on particular chemical reactions or rates. GRImech 2.11 was compared with the reduced Methmech in order to test the significance of the more complex nitrogen chemistry involving N_2O and NO_2. This chemical flexibility could be very useful for modeling other fuels, additives or controls which might be postulated to control NO emissions. Prediction accuracy is good enough, especially for developing trends, to add significantly to a development program for NO emissions reduction. Altering burn rates helps to approximate different swirl intensities and cylinder head designs which are costly and time consuming in an experimental setting.

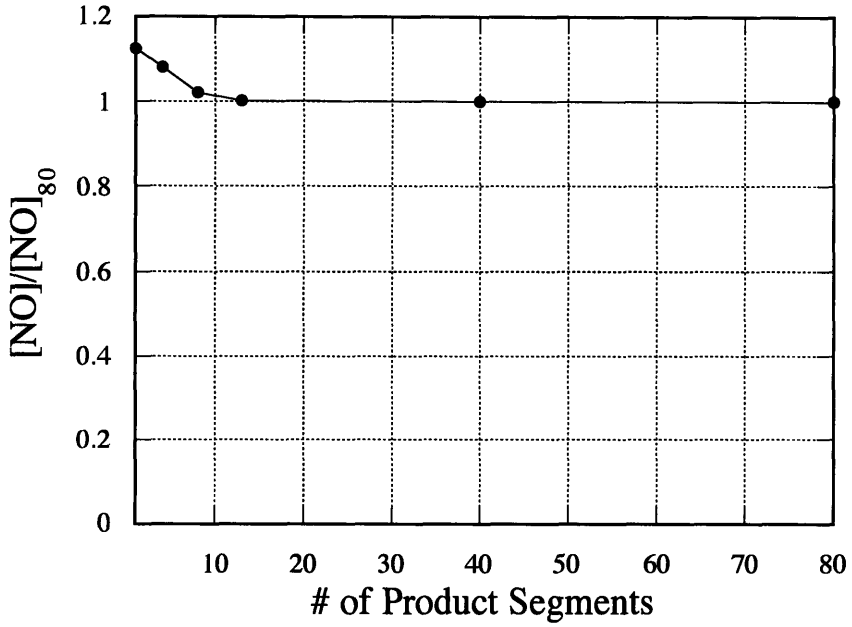

Figure 3.1 NO prediction's dependence on number of product segments.

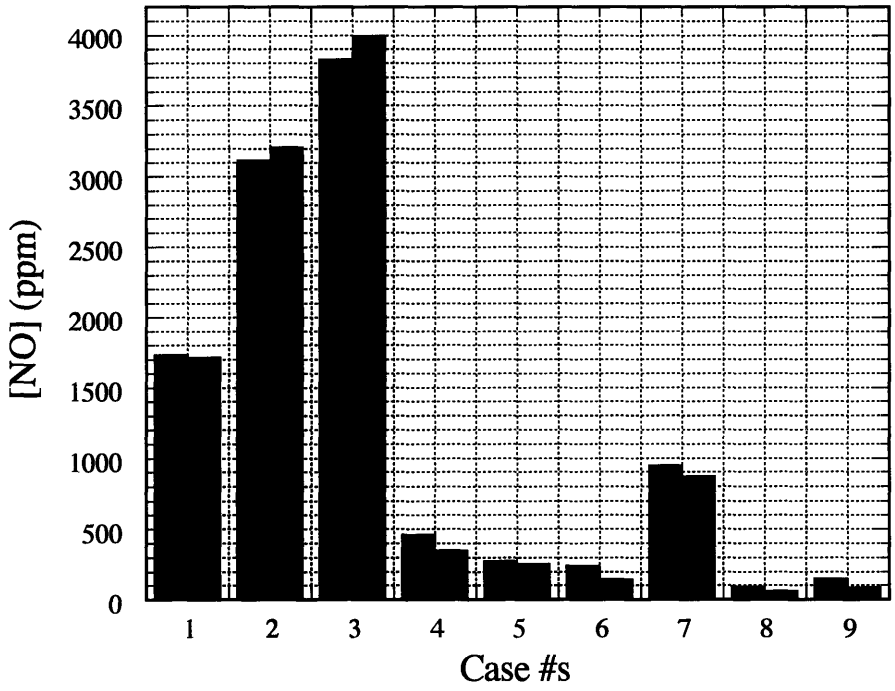

Figure 3.2 COOK predictions (second bar) compared with the experimental measurements (first bar).

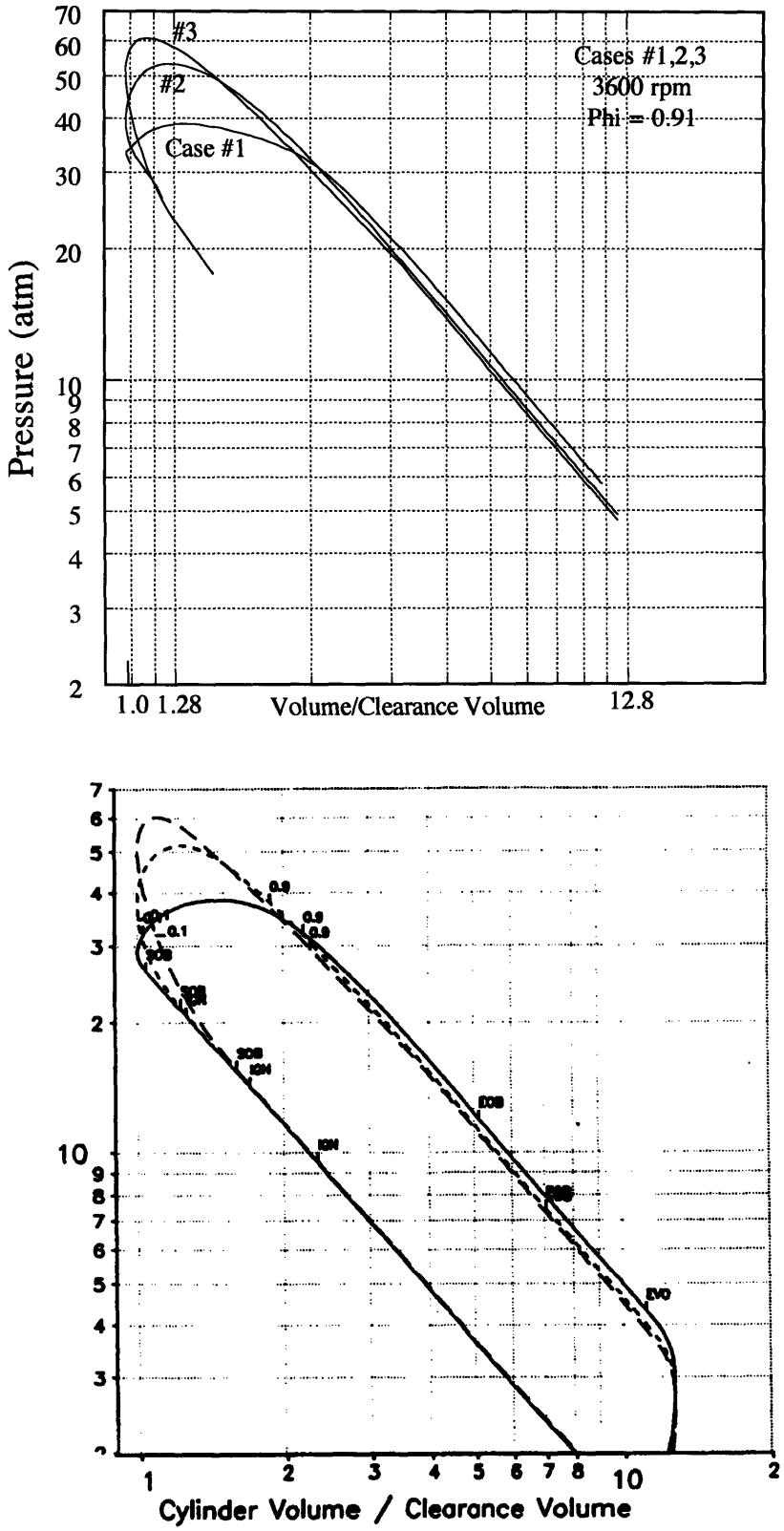

Figures 3.3 and 3.4 Comparisons of the actual pressure traces (bottom) to COOK's predicted pressure traces (top) for the experimental cases #1,2 and 3.

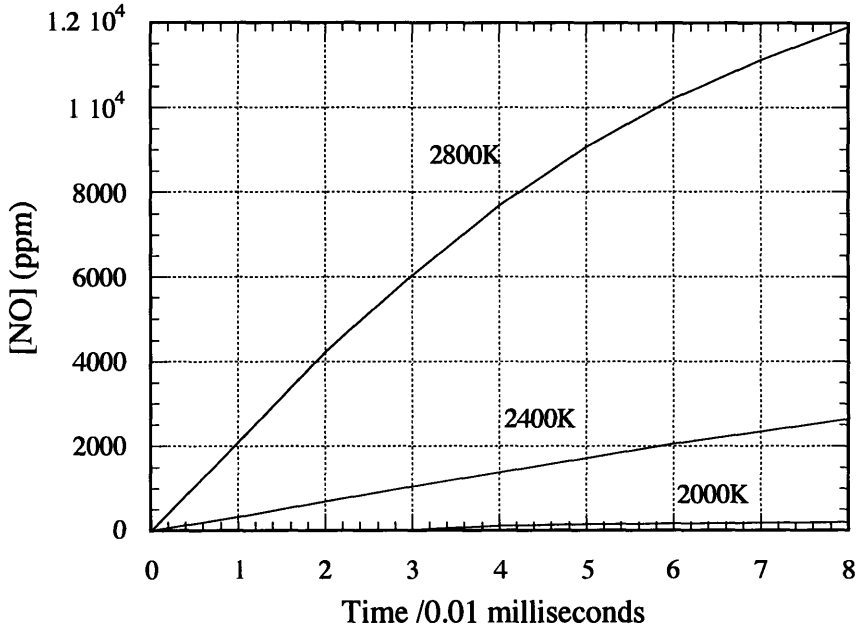

Figure 3.5 NO formation kinetics' high dependence on temperature.

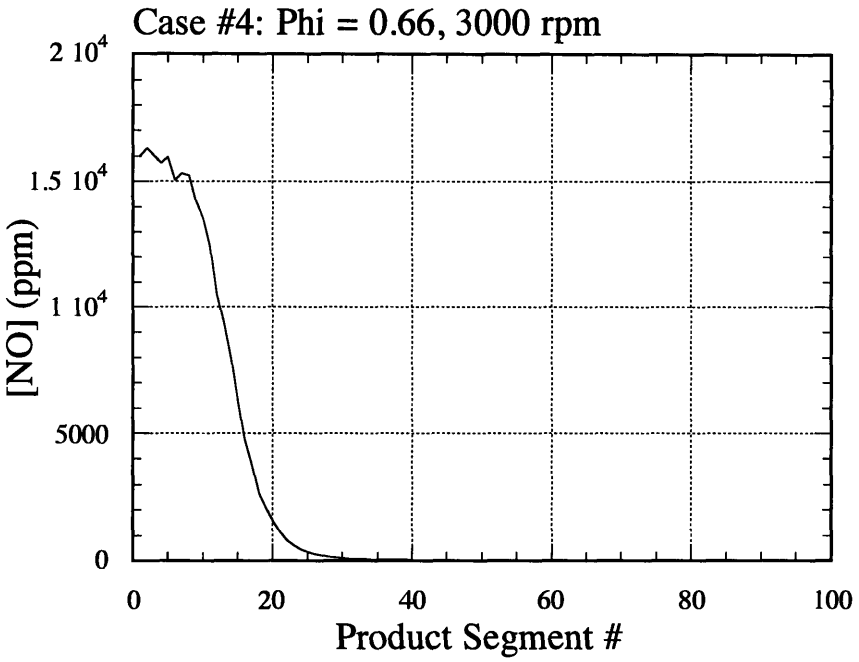

Figure 3.6 The concentration of NO in the different product segments at the end of expansion.

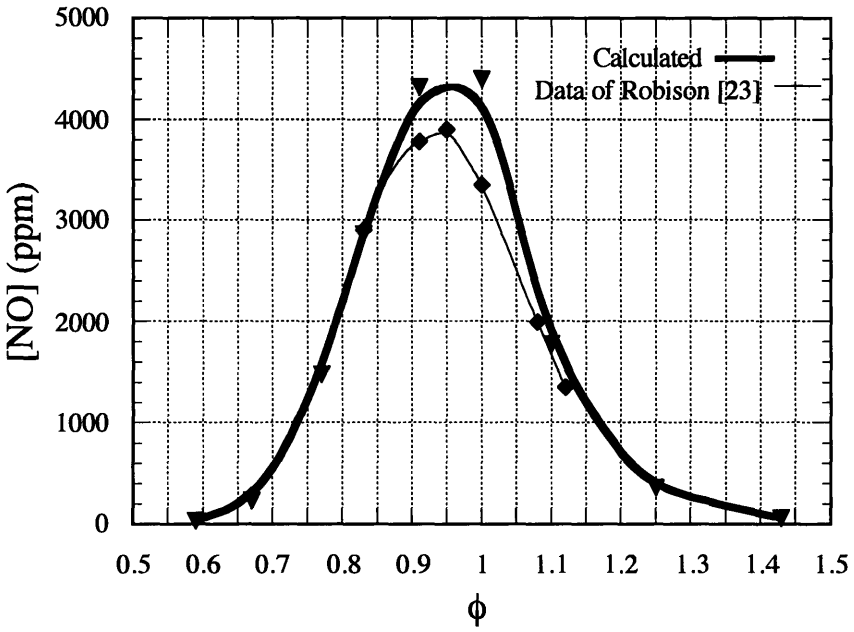

Figure 3.7 NO versus fuel/air equivalence ratio comparing COOK model results to data from Robison as presented in Blummer et al[23]. Note that the fuel and engine conditions were different in the Robison runs and that this comparison is made to illustrate the similarity in the shapes and locations of the [NO] emissions peaks.

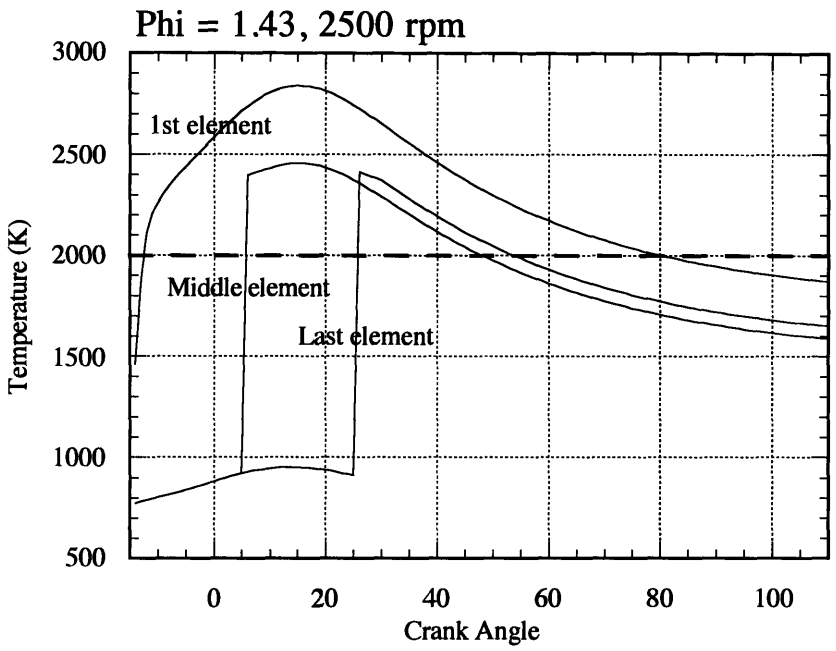

Figure 3.8 Temperature histories for several product elements.

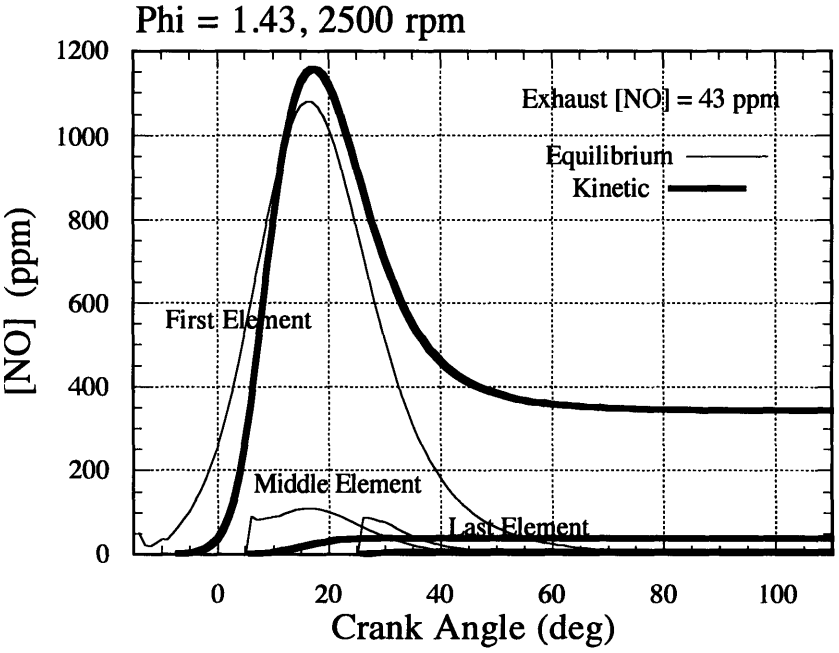

Figure 3.9 NO concentration histories for several product elements.

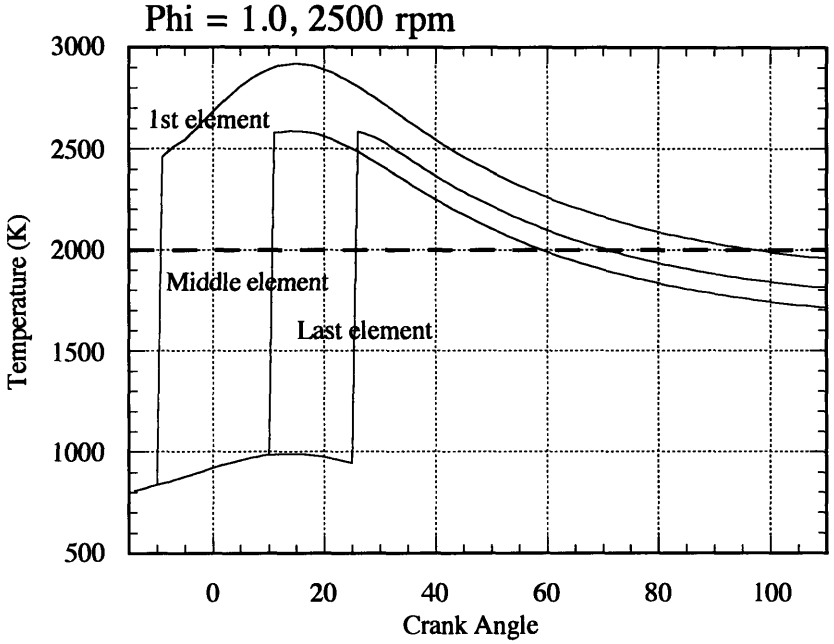

Figure 3.10 Temperature histories for several product elements.

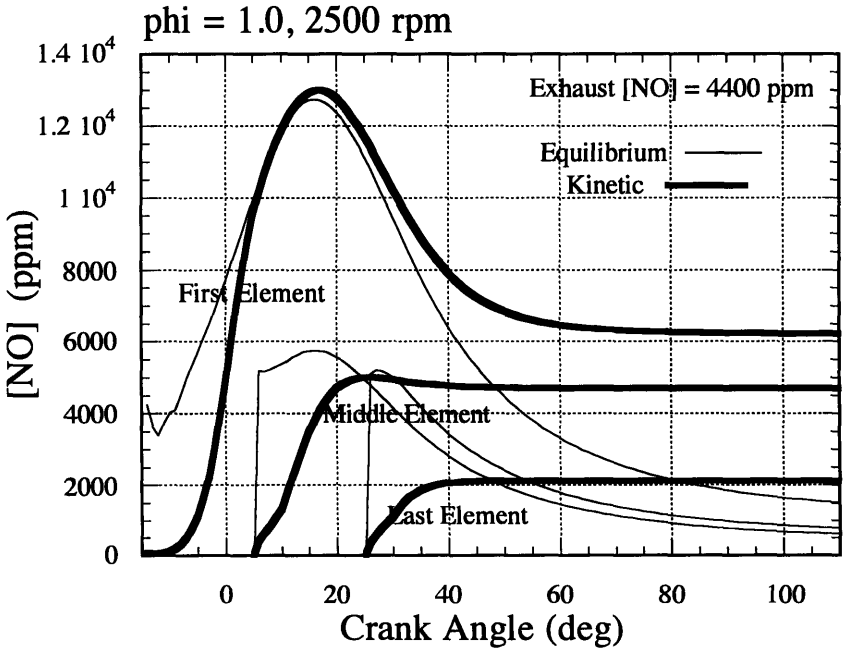

Figure 3.11 NO concentration histories for several product elements.

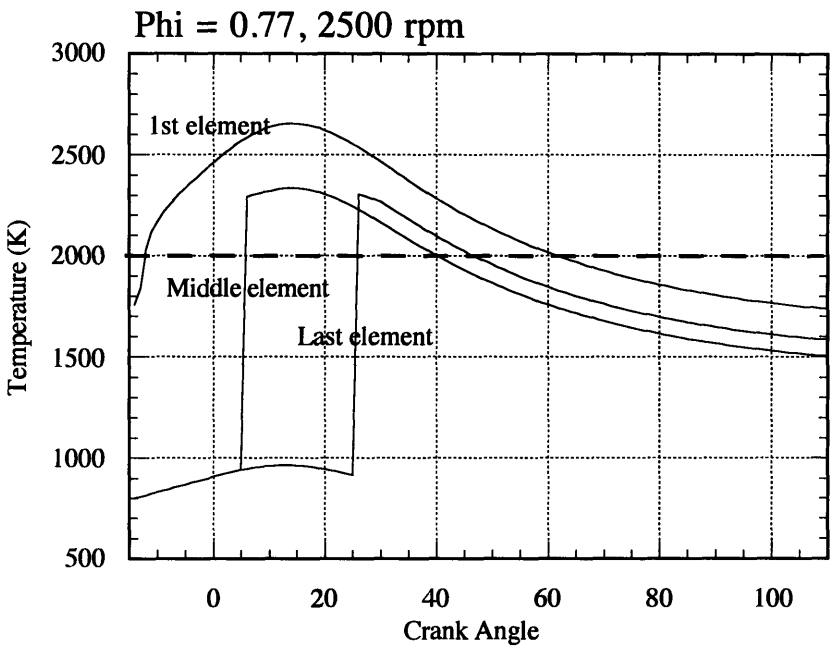

Figure 3.12 Temperature histories for several product elements.

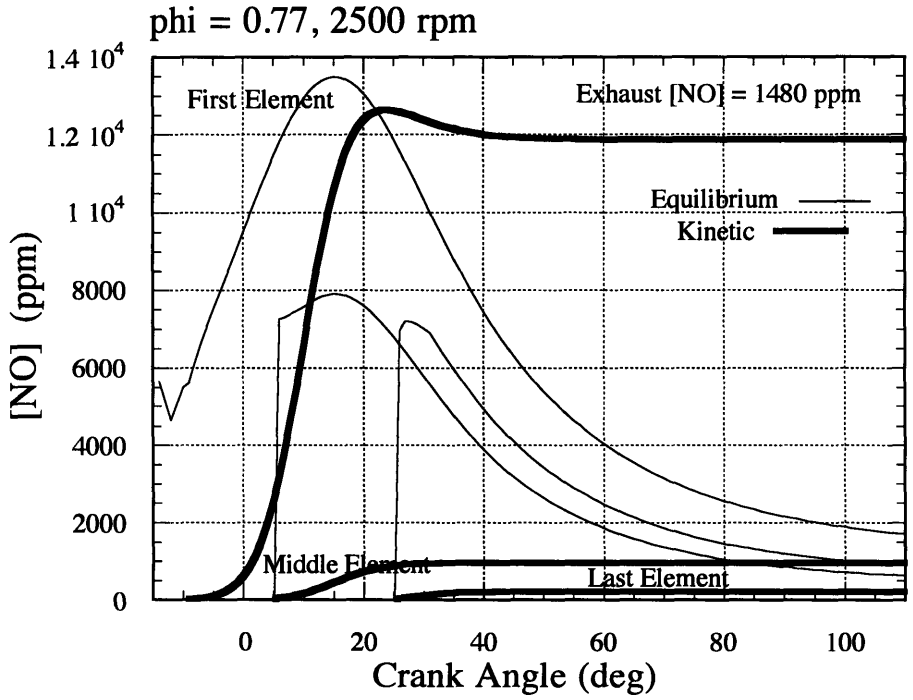

Figure 3.13 NO concentration histories for several product elements.

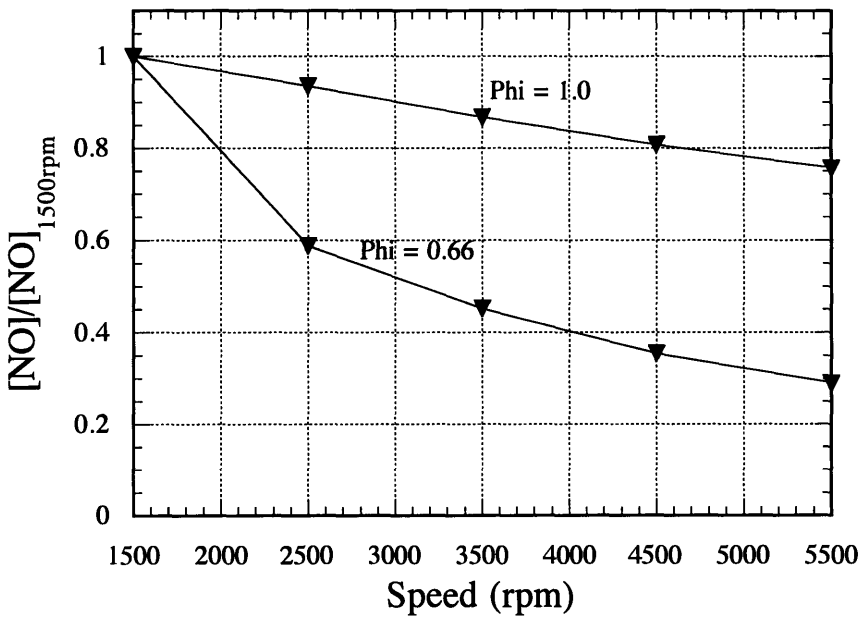

Figure 3.14 Different NO formation mechanisms make lean engines very sensitive to time scale changes.

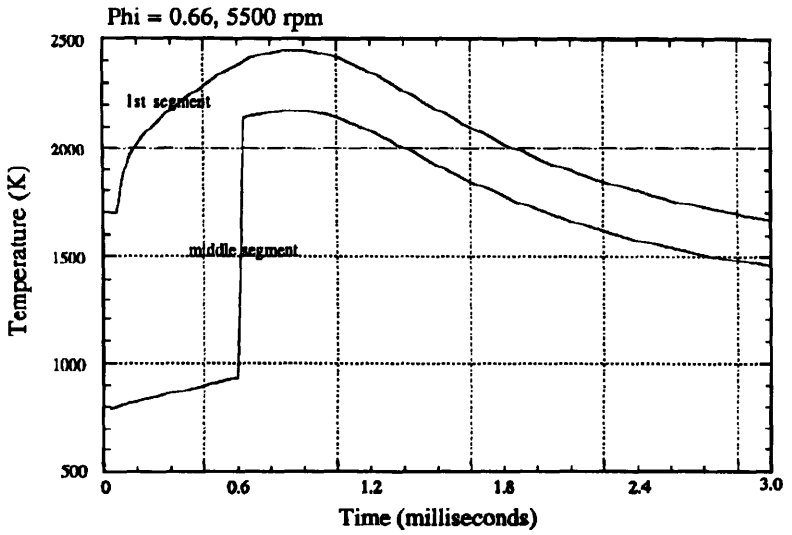

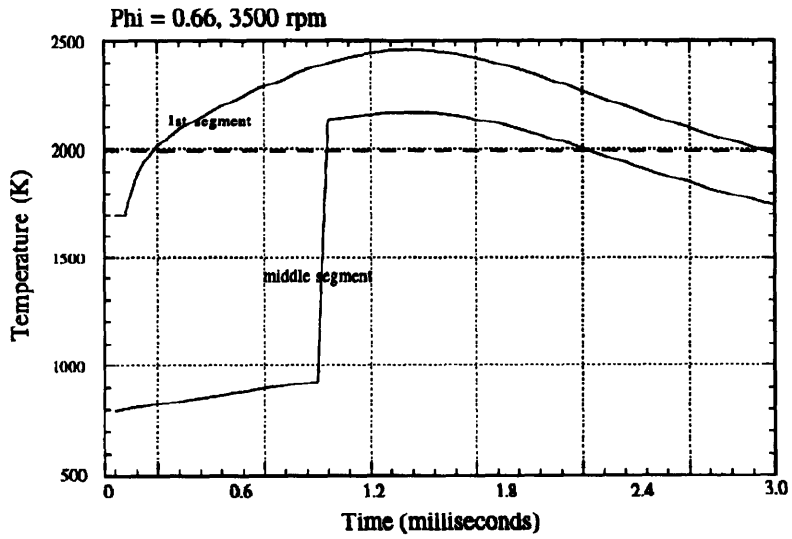

Figures 3.15 and 3.16 Temperature versus time for several product segments at different engine speeds.

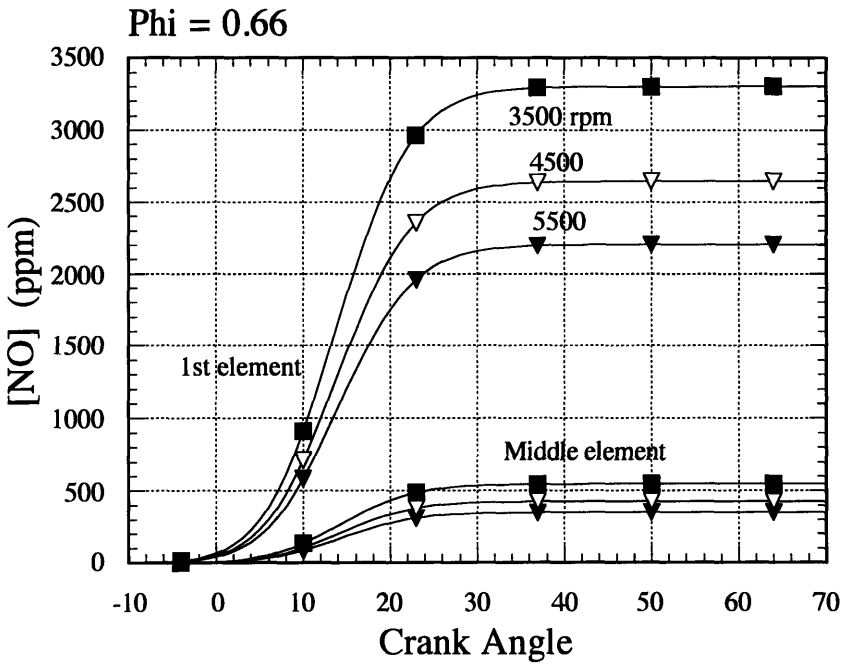

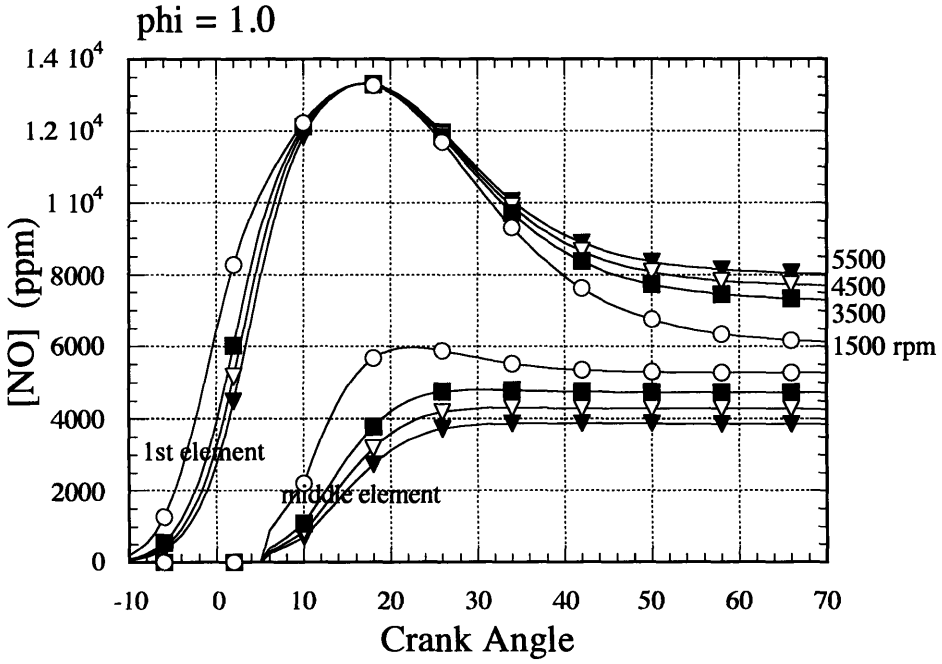

Figures 3.17 and 3.18 NO histories for several products at different speeds for a lean and stoichiometric case.

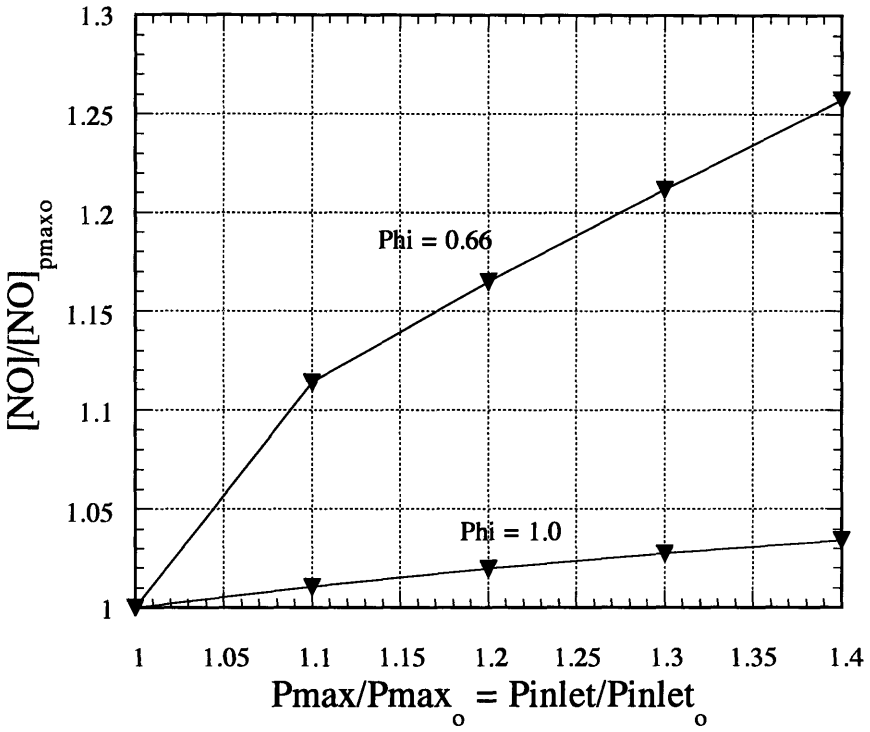

Figure 3.19 Another example of lean engines' sensitivity to temperatures

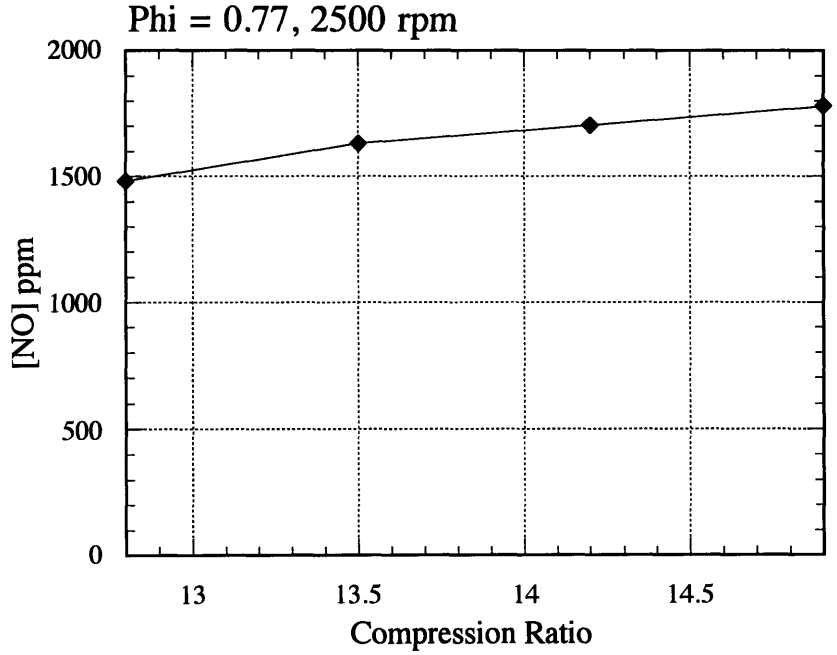

Figure 3.20 NO emissions versus compression ratio.

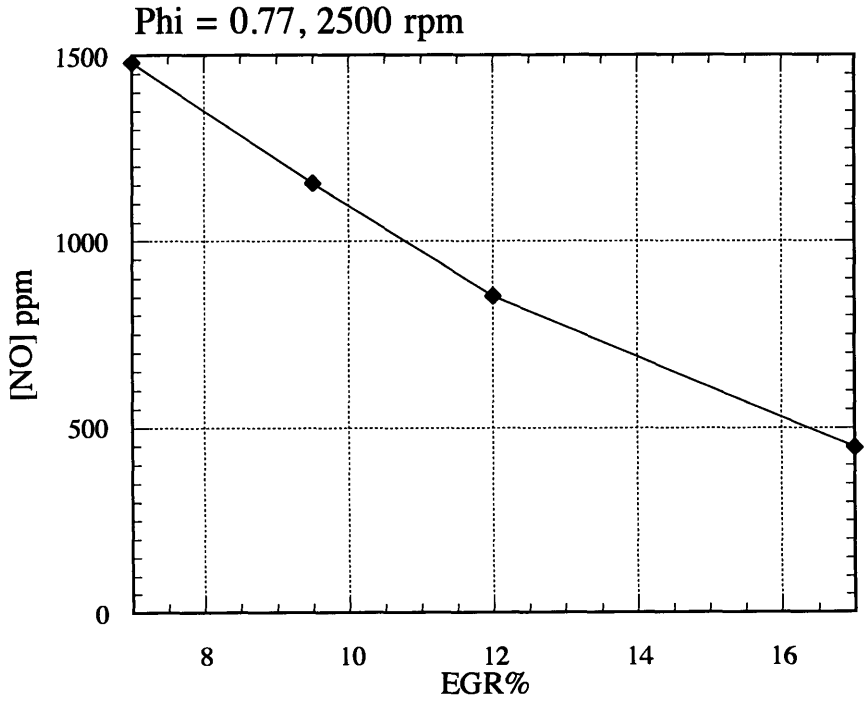

Figure 3.21 NO emissions versus EGR levels.

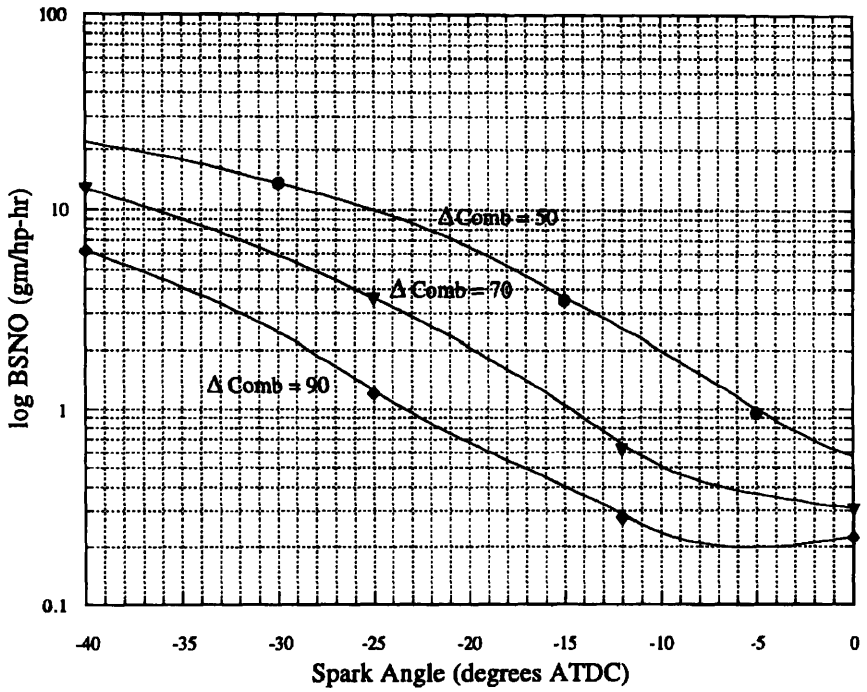

Figure 3.22 Brake Specific NO emissions as a function of both combustion duration and the location of the spark in the cycle.

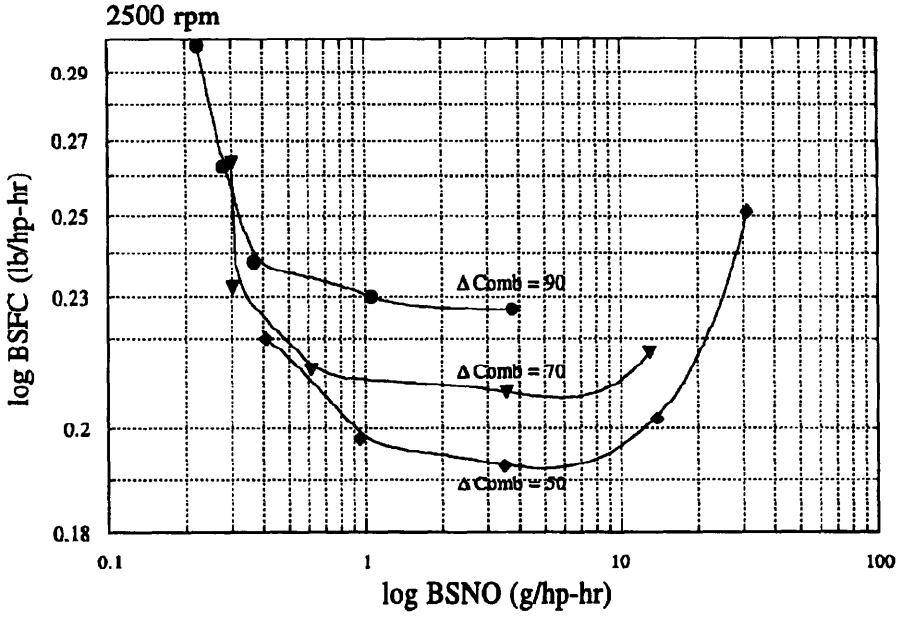

Figure 3.23 Relationship between brake specific NO emissions and fuel consumption, where each curve is made by changing the spark timing.

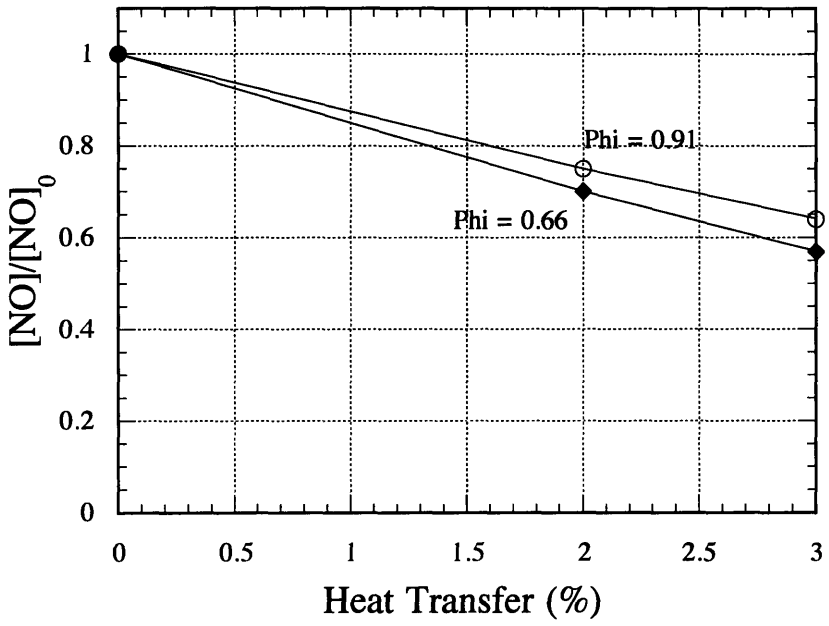

Figure 3.24 NO emissions versus heat transfer as a fraction of the bulk total energy deposited in the cylinder.

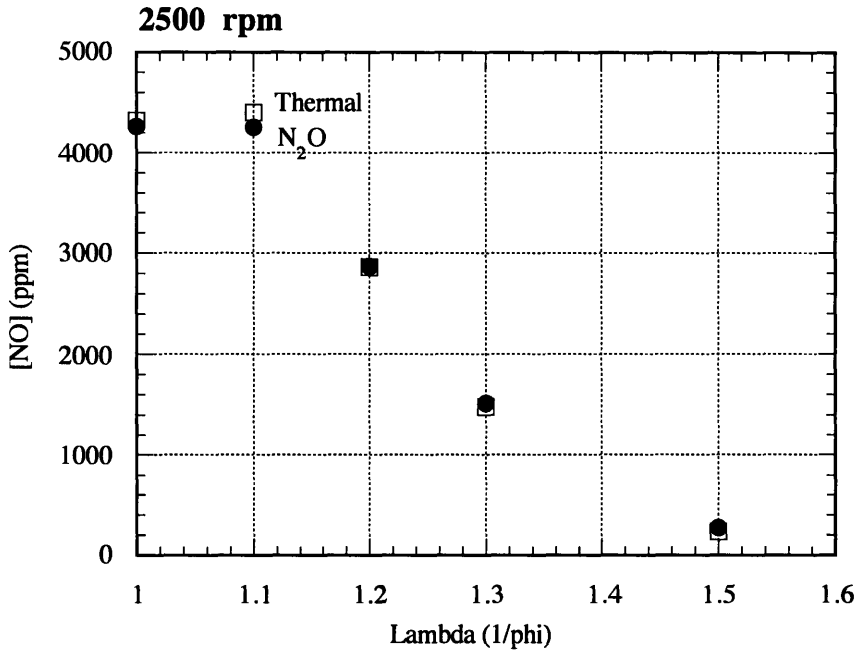

Figure 3.25 NO emissions modeled using a thermal only mechanisms and a more detailed N_2O-including mechanism from GRImech 2.11.

4. CO Emissions Modeling

4.1 Introduction

One goal of constructing the COOK model was to predict the level of CO emissions from lean natural gas engines. CO levels are relatively low in the exhaust of lean engines because of the lack of excess carbon, but are orders of magnitude higher than the equilibrium levels at the exhaust conditions. The high CO levels are thought to result from both chemical quenching as well as from wall and crevice interactions. In this chapter, experimental data from gas engines are analyzed to provide some additional insight into CO emissions mechanisms. Predicting CO emissions using COOK will then be discussed as well as more general aspects to modeling CO emissions.

4.2 CO Emissions Mechanisms

CO oxidizes by a complex set of reactions involving carbon, hydrogen and oxygen where the dominant reactions are:

With low activation energies, the CO reactions are very fast at temperatures above around 1200°K. Figure 4.1 shows the integration of the CO to CO_2 oxidation at different temperatures. Above 1200°K, CO is brought quickly to its equilibrium but as the temperature falls, like NO, so do its equilibrium values and its rate of oxidation. Eventually, CO oxidation reactions become frozen, leaving CO in the product element at a level above its equilibrium value.

The importance of freezing to CO emissions is very different from that for NO emissions. NO is being formed from zero and thus, the later colder elements will have very low NO concentrations, as is shown in figure 3.6. CO is oxidized from a finite level within the flame zone, and colder elements will not oxidize CO to CO_2 very effectively. Experimental measurements of local CO concentrations show that CO exists substantially among the colder 'quench layer' gases which lose heat to the cylinder walls [22]. These quench layers either do not burn outright or burn very slowly and freeze while CO concentrations are still very high.

Some of the experimental data used in the development of COOK seemed to add more evidence to support this wall quenching mechanism. Wall quenching has been implicated as the major source of hydrocarbon emissions in gas engines [33, p245]. As the flame encounters the wall and the gases cool, burning is impeded and local extinction occurs. Here, combustion is incomplete yielding heavy concentrations of flame intermediates like hydrocarbons and CO. This CO source has been shown to be significant in gasoline engines as quoted in Heywood, but for lean gas engines specifically, this mechanism had not been explored. The data used to develop COOK contains NO, CO and unburned hydrocarbon emissions. Comparing them can show how CO and hydrocarbons are formed via related mechanisms. Figure 4.2 shows data from a set of experimental measurements for different cylinder head designs and figure 4.3 for different spark timing for the same head builds. The different head designs induce different swirling motions and compression ratios but as can be seen, do not effect the overall CO and HC emissions as they are virtually identical. It is the same story with the different spark timings in figure 4.3. Here again, the pressure and temperature histories do not effect CO emissions, as the three timings yield virtually the same CO emissions.

Figure 4.2 and 4.3 strongly suggest that CO emissions are dependent on the same dominant mechanism which controls HC emissions. CO and HC emissions rise in similar manner over the entire lean region. HC emissions are evidently more sensitive to changes in equivalence ratios, but this is irrelevant to the point being made. It is clear that flame-wall phenomena become pronounced at leaner equivalence ratios and this increases quenching effects, and HC and CO emissions. This data shows that accurate CO emission modeling should place great emphasis on flame-wall interactions.

Other possible sources for CO emissions, though much less significant, are local variations in Phi due to poor mixing. These would have two effects. Rich 'spots' would leave high CO concentrations simply from their inability to supply enough oxygen even with a high temperature

history. On the other hand, very lean spots which form later in the cycle would be prone to early freezing of the CO oxidation reactions much like the wall layer, leaving excess unoxidized CO in the exhaust.

4.3 COOK's Predictions

COOK was used to predict CO emissions for the 9 cases covered previously in the NO chapter. Comparing the experimental and predicted values, the importance of the CO mechanisms missing from the COOK model is obvious.

Table 4.1 CO comparisons

Case#	ϕ	CO emissions (experiment ppm)	CO emissions (predicted ppm)	%Difference
1	0.91	316	55	82.5
2	0.91	307	28	90.9
3	0.91	307	34	88.9
4	0.67	490	4.7	99.0
5	0.67	490	3.2	99.3
6	0.68	507	9.0	98.2
7	0.65	626	2.6	99.6
8	0.65	463	2.7	99.4
9	0.63	696	1.7	99.7

The initial formulation of the COOK model was geared towards predicting NO emissions. The transition from reactant to product was modeled as an equilibrium state of the reactants for numerous products, including CO and CO_2. This model was logical for the NO predictions, since even in these lean engines, pressures are high and flame zones are fairly thin among those early burned segments most important to NO formation. Note that the differences between the CO predictions for the rich and leaner cases in table 4.1 reflect the higher CO equilibrium values of the richer conditions.

Temperature and CO histories are presented in figures 4.4 to 4.7 for a stoichiometric and lean case to illustrate the equilibrium and kinetic processes happening within the products. As is shown, the temperatures are high enough among the products to effectively keep CO at its equilibrium state throughout most of the cycle.

Figures 4.8 show CO emissions for a range from lean to rich along with a comparison with data found in Heywood [11]. Here, the rich regimes are largely underpredicted much like the lean regimes before. Since the rich regimes are much like the lean regimes in that temperatures are low and wall quenching is pronounced, the lack of wall quenching is a major factor in the discrepancy

between the data and COOK's predictions. Notice that as wall phenomena increase in significance as the phi is moved greater and greater away from 1.0, the difference between the COOK predictions and the experimental data rises.

Note that the discrepancy between the predicted and experimental emissions are least at near stoichiometric. This also supports the thesis of the significance of flame-wall quenching as quenching is minimized at stoichiometric operation because of higher temperatures, faster flame speeds and higher pressures. This is also seen in the data in figures 4.2 and 4.3, where the HC and CO emissions are at a minimum around stoichiometric conditions.

To possibly improve the model, some additional mechanisms were added and will be discussed next.

4.4 The Mid-Flame and 2 Step Combustion Initial Product State.

Near the wall or within leaner regions in an imperfectly mixed charge, the temperatures or pressures are lower, slowing the reactions and widening the flame zone. Under these conditions, the equilibrium composition might not be a good model for the initial product state. Figures 4.9 and 4.10 show qualitatively how the flame is affected by pressure and how, for the 1 atmospheric flame, equilibrium occurs much later than for the higher pressure flame.

The equilibrium combustion model had assumed CO has burned out to CO_2 in the flame and had reached equilibrium. Thus, product elements *start* with little CO and have none to oxidize. Using this model, colder or locally lean spots which might be hindered in their CO oxidation would have no CO to oxidize and the possibility of freezing from the initial high CO composition is lost.

To facilitate a more robust initial product state, two mechanisms were added to the COOK model:

1. Two-Step Transition: the transition as an equilibrium state without CO_2, thus making the combustion transition a two step process: one, where the flame burns to CO and two, where the products oxidize the CO to CO_2.

2. Mid-flame transition: a premixed flame code solves for the concentration profiles through the flame zone and takes a 'slice' of the species and temperature at a point within the flame, as illustrated qualitatively in figures 4.11 and 4.12.

Neither the mid-flame nor the two-step models reduced the discrepancy between the experimental data and the predictions. Figure 4.13 compares the two step transition and the standard equilibrium transition on the CO histories. To further elucidate the point, a run was done at $\phi = 0.55$ with a low initial temperature and pressure, but still the kinetics were fast enough to oxidize CO out and make the two step transition and the equilibrium transition equal (figure 4.15). Most of the CO present in the products initially (as the products' initial state) have burned out within a few, or at most, 10 crank angles.

4.5 Adding a Spatial Dimension: Unmixidness

In the engine's reactant mixture there are spatial variations in the level of mixing which has occurred between the fuel and air. Fluid motion can isolate portions of the chamber from mixing, leaving spatial gradients in ϕ. This process may influence the overall CO emissions in 2 ways:

1. by causing rich spots to produce residual CO from the carbon excesses

2. by causing lean spots whose CO oxidation reactions would quench from low temperature, especially those burning late in the combustion phase.

A mechanism for adding these lean and rich spots at random was added to COOK in hopes of modeling the CO residuals which supersede those predicted earlier. To introduce these variations in ϕ, an unmixidness routine was added to facilitate a standard distribution of ϕ around some average ϕ. Here, the degree of unmixidness, s, was specified,

$$s = \frac{\sigma_\phi}{\bar{\phi}}$$

where σ_ϕ is the standard deviation of ϕ around its mean, $\bar{\phi}$.

As each Δm is prepared for its transition to its initial product state, its ϕ is determined by a Gaussian random number generator. A typical set of ϕs for a run is shown in figure 4.16. Figures

4.17 and 4.18 show the distributions for an s of 0.18 and 0.02. Figure 4.19 shows that the pressure trace for the model is unaffected by the distribution when compared to a run with no variation in ϕ.

Mixing levels in engines are hard to estimate and measure. Since the values of s is unknown in the engines and under the conditions being modeled, the treatment of the results from this study will be purely qualitative. The effects of unmixidness on COOK's predictions for case #4 is shown in figure 4.20. It can be seen that CO emissions increase greatly with increasing variation of ϕ which produces enough CO to match the actual CO measured in the engine.

A close analysis of the results show that most of the additional CO from the unmixed runs are from richer regions and not from the freezing of the colder, leaner regions as might also be expected. Figures 4.21 and 4.22 show that the additional CO in the predictions come mainly from the rich segments. Figure 4.23 shows more closely how, while the later elements freeze CO at higher levels, the richer spikes cause most of the additional CO in the predicted exhaust. Also, the first burned segments contribute too much to the final CO which is not in accordance with other researchers' conclusions. From these results, it is clear that rich spots could potentially contribute significantly to the overall CO emissions in a poorly mixed engine. Some jet engine combustors have an overall unmixidness level, s, of close to 0.2, which would greatly contribute to higher CO emissions.

Unmixidness in gas engines is hard to measure and is probably fairly low. The CO emissions resulting from low unmixidness, as shown in figure 4.20 are fairly low. This is in agreement with the findings of other researchers that most of the CO emissions originate from the wall quenching layer and not significantly from scattered regions throughout the cylinder. Estimating the S of gas engines to be less than 0.1 would put CO emissions from unmixidness at about a few percent of the overall CO emissions.

4.6 Conclusions

Experimental data clearly shows the significance of flame-wall interactions in CO emissions. The similarity in HC and CO emissions over a range of operating conditions show that the quenching of later, colder mixture elements are important to CO exhaust levels and must be included in any detailed model of CO emissions. As operating conditions become leaner, CO emissions grow as the significance of these wall phenomena increase under colder and more unstable combustion

conditions.

COOK, being built around a zero dimensional thermochemical model lacks the facility for modeling spatial phenomena which would enable it to model the late flame wall interactions serving as the driving mechanisms behind CO emissions in lean engines. Contrasting the predictions with the experimental data show how important the flame wall interactions are and how their influences change with the equivalence ratios. The flame model was changed to enable freezing of CO from an initially higher point 'within' the flame zone, which did not prove to reduce the discrepancy between COOK's predictions and the experimental data. Adding random variations in the fuel air ratio of the gas elements shows how local rich sport could contribute a few percent in a well mixed engine or more significantly in a poorly mixed one.

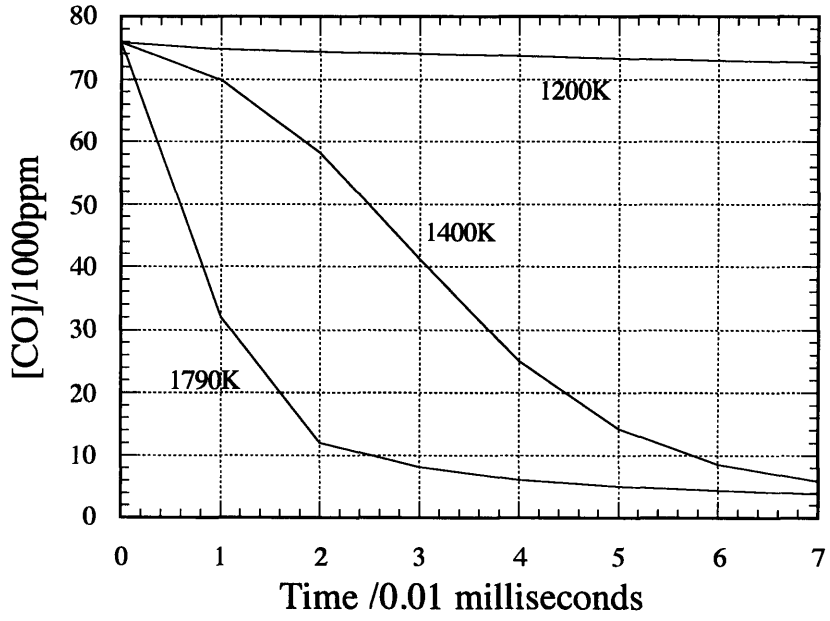

Figure 4.1 The CO oxidation rates show strong dependence on temperatures above 1200°K.

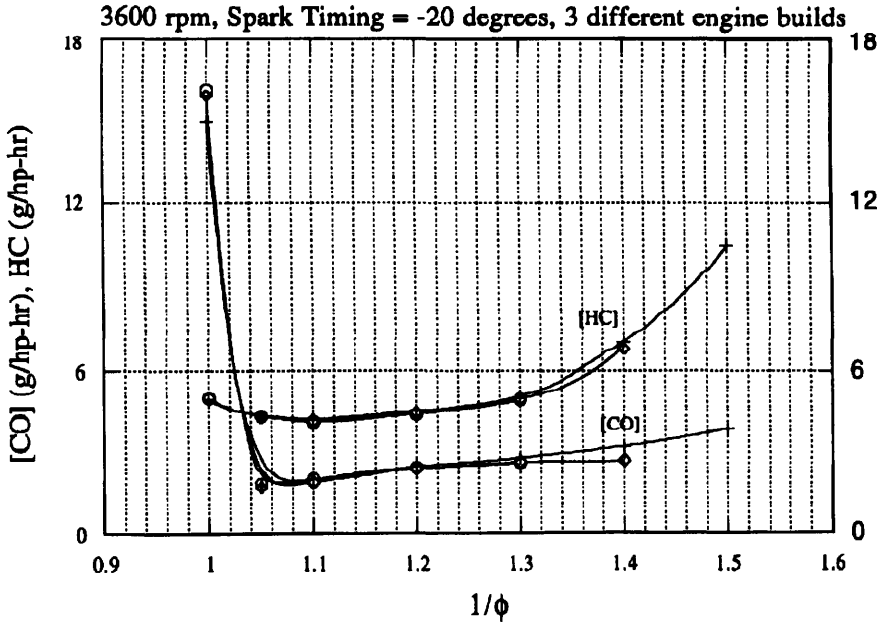

Figures 4.2 HC and CO emissions over a range of equivalence ratios (experimental data). The three curves are for different engine builds.

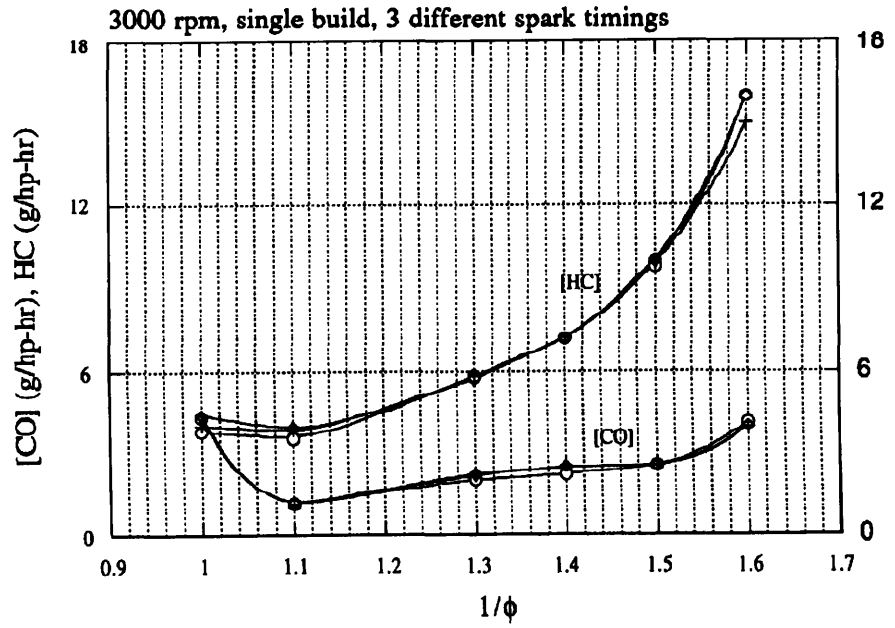

Figures 4.3 HC and CO emissions over a range of equivalence ratios (experimental data). The three curves are for different spark timings.

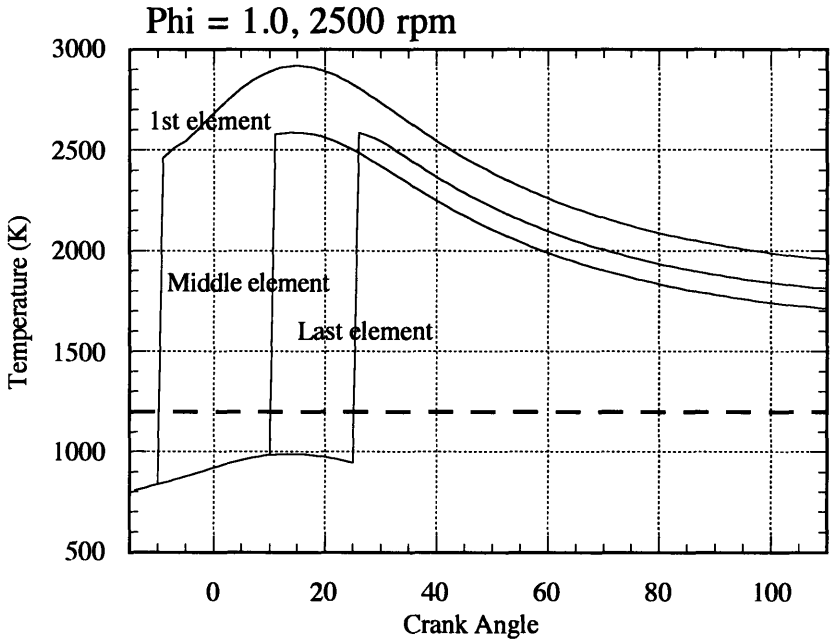

Figure 4.4 Temperature histories for different product elements.

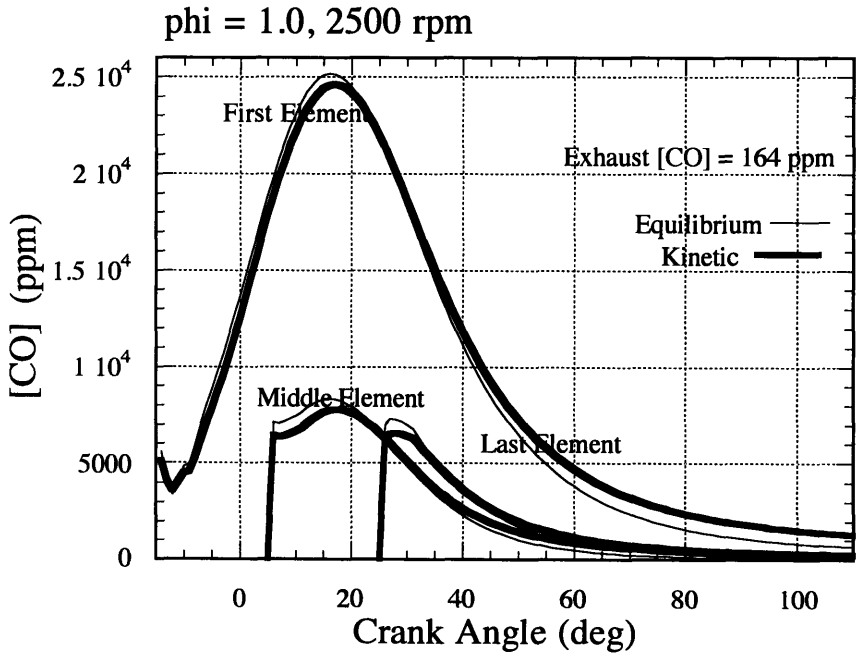

Figure 4.5 CO histories for different product elements.

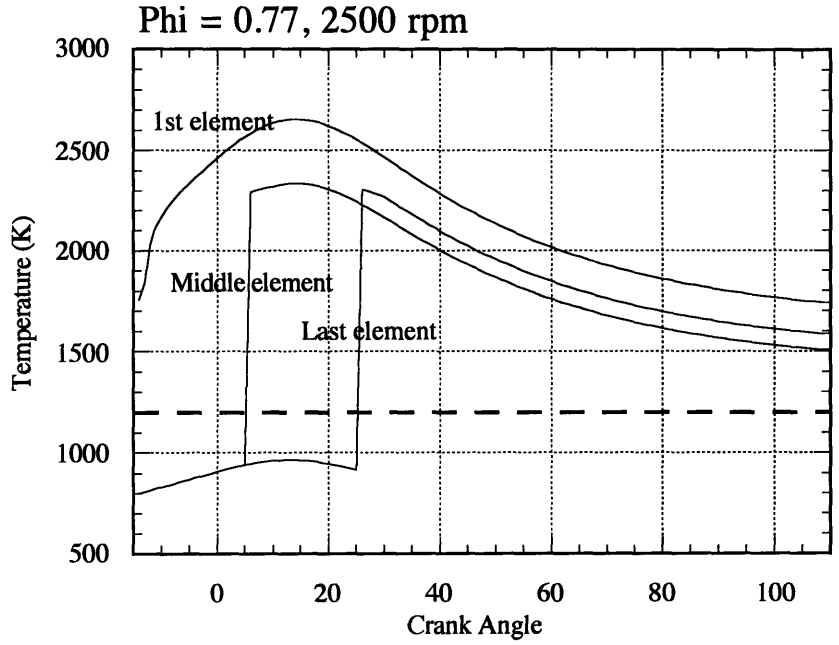

Figure 4.6 Temperature histories for different product elements

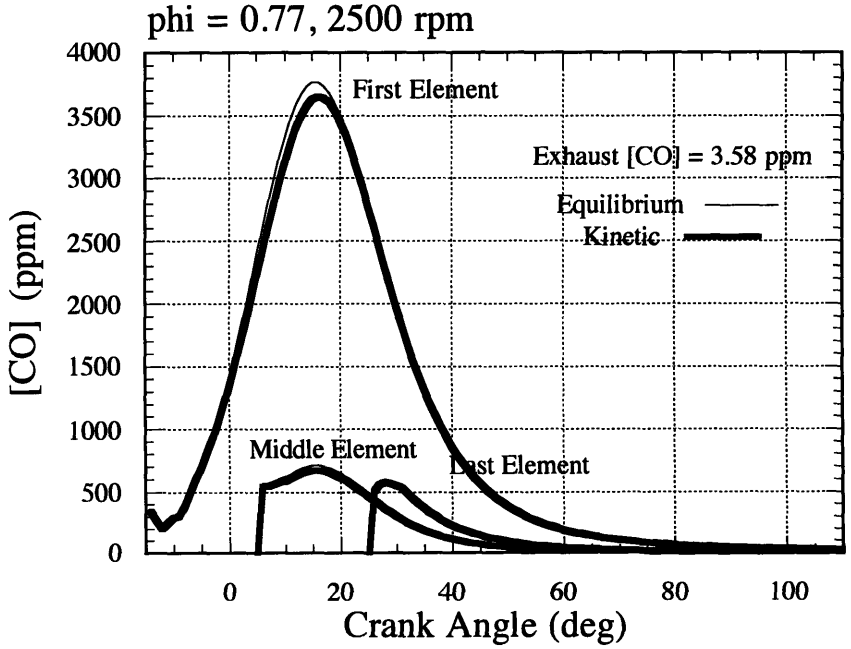

Figure 4.7 CO histories for different product elements.

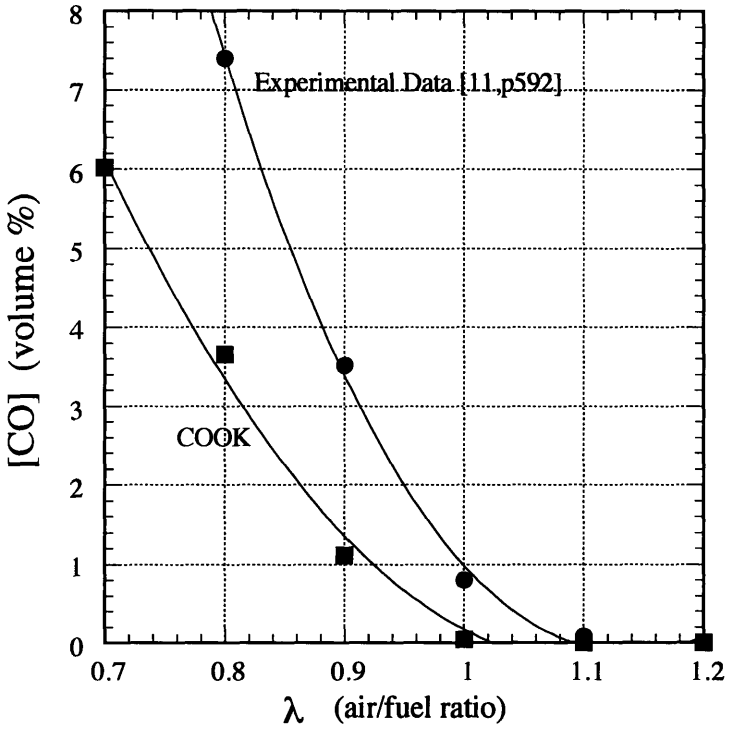

Figure 4.8 Comparing COOK predictions and experimental data over a range of equivalence ratios.

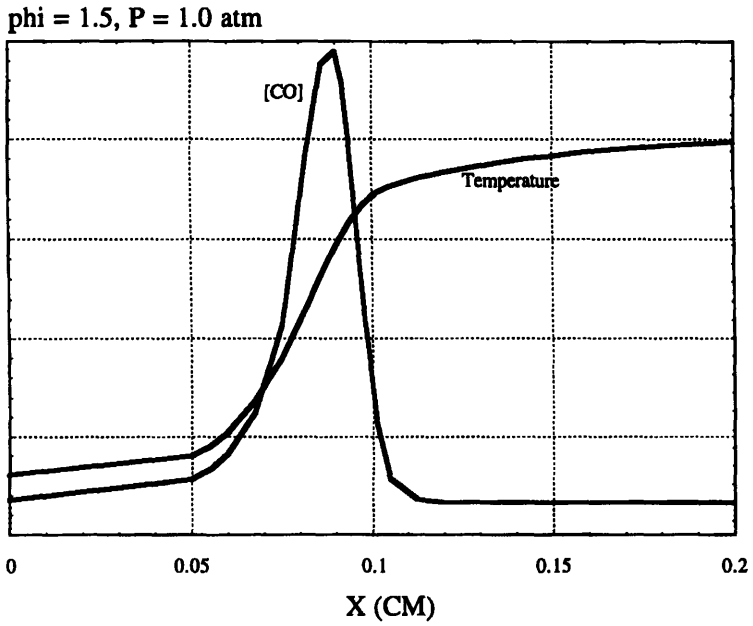

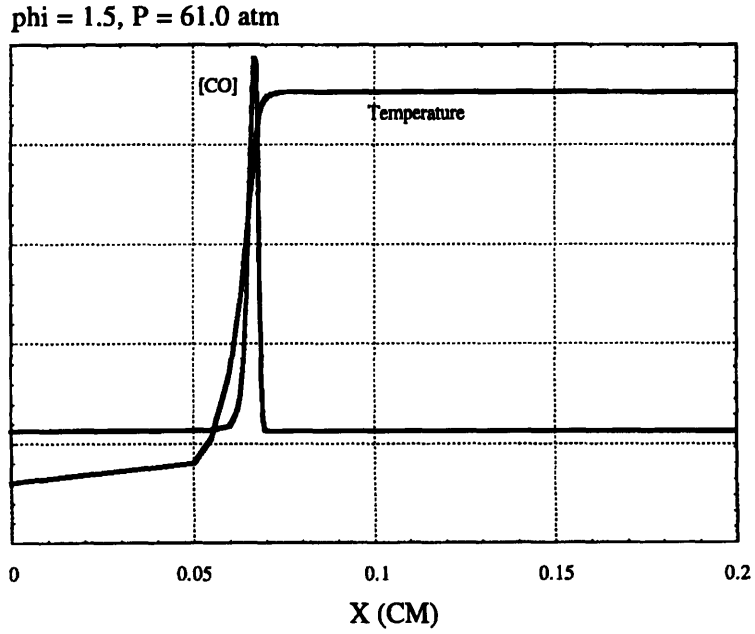

Figures 4.9 and 4.10 Flame profiles showing CO formation and oxidation within the flame zone for a 1 and 61 atmosphere flame illustrating the difference in flame thicknesses.

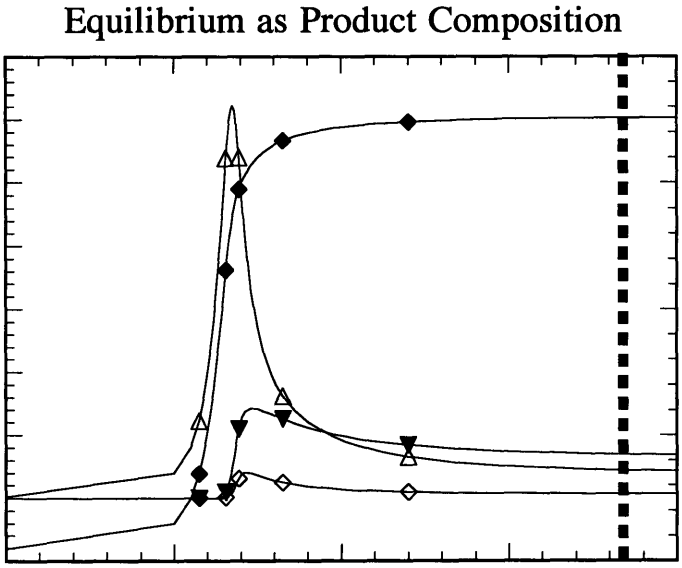

Figure 4.11 A typical flame profile showing qualitatively how the equilibrium model extracts the flame composition at a point behind the flame where equilibrium has been reached among the major products of combustion.

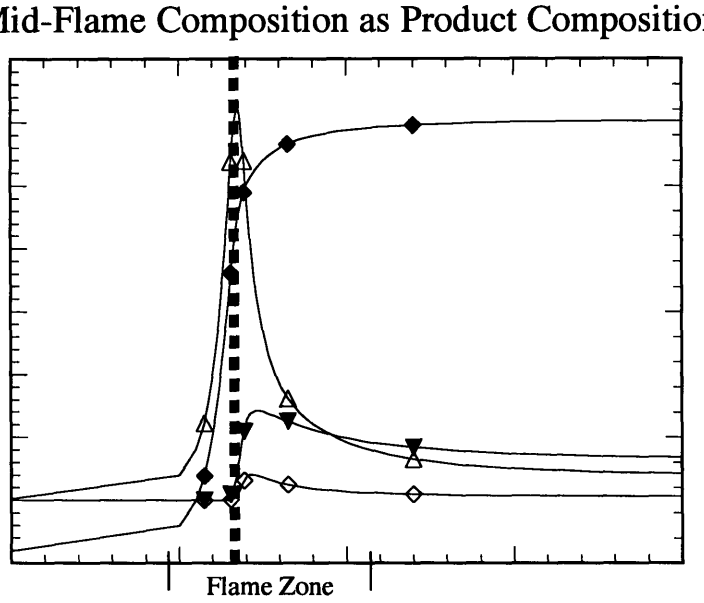

Figure 4.12 A typical flame profile showing qualitatively how the mid flame model extracts the flame composition at a point within the flame zone.

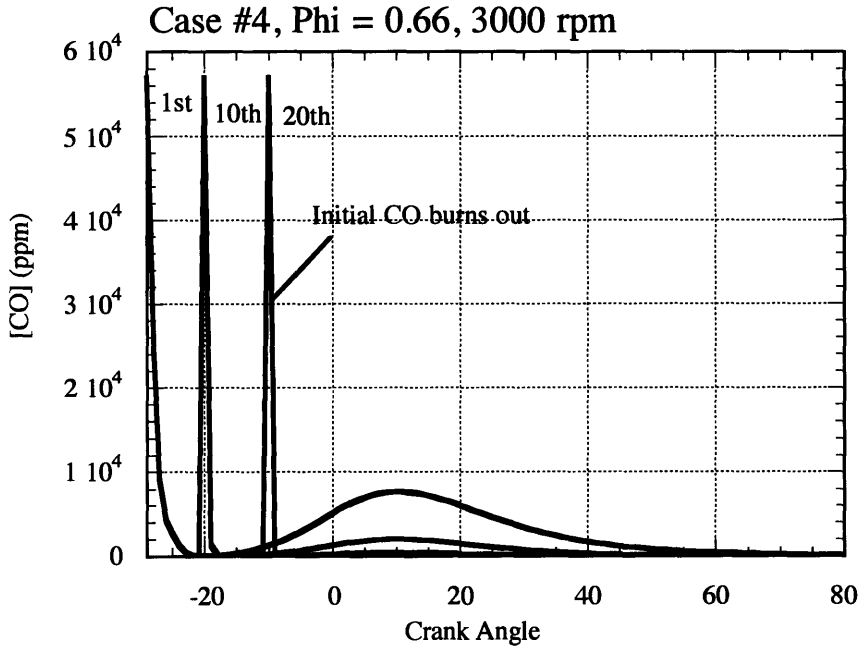

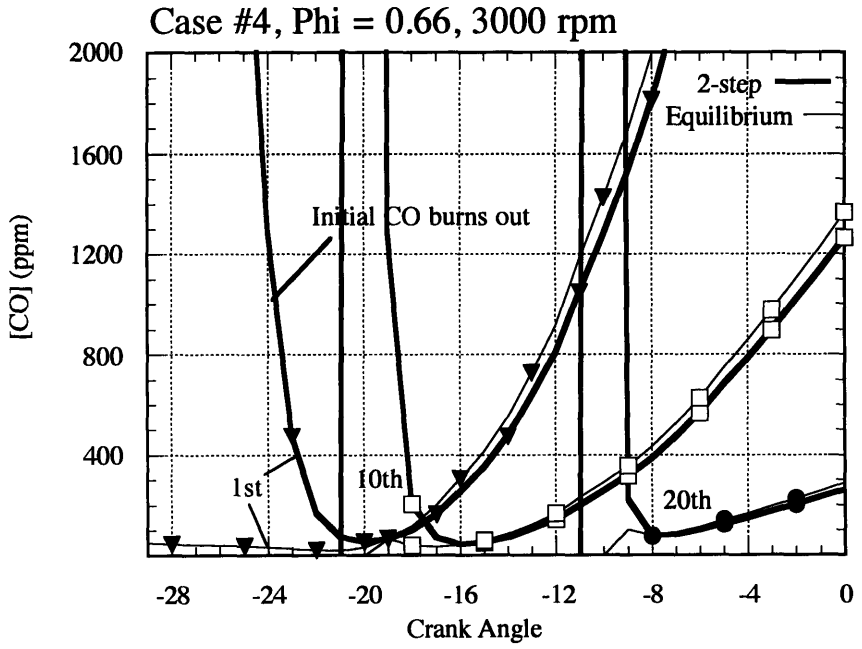

Figures 4.13 and 4.14 Comparing the two step transition to the equilibrium transition showing how CO oxidizes quickly enough to make differences between the two models insignificant. 4.14 is a close up of the starting region of figure 4.13. The spikes are from the high initial CO concentrations.

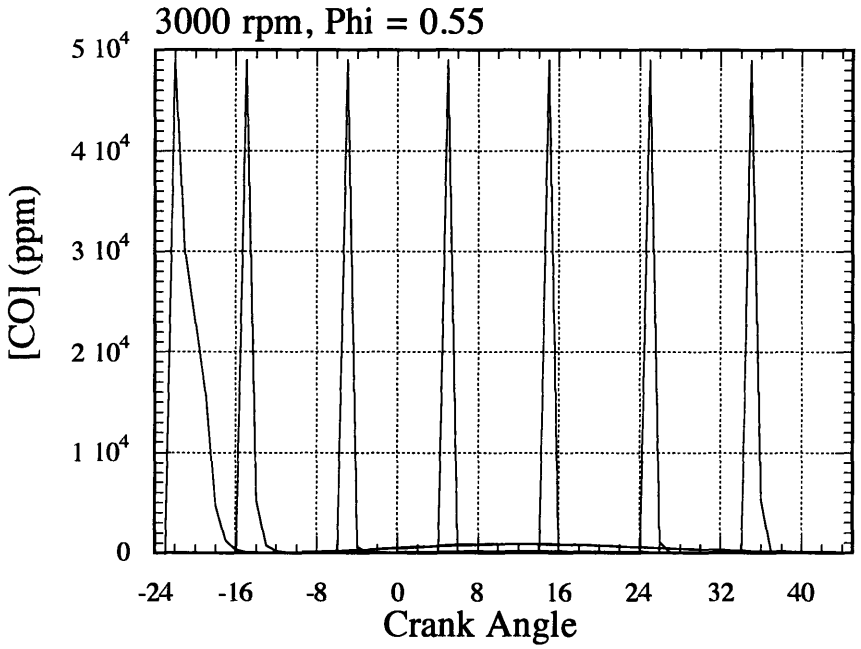

Figure 4.15 The CO histories for product segments at every 10 crank angles are plotted, showing how even at very low equivalence ratios, the CO-CO_2 system will equilibrate.

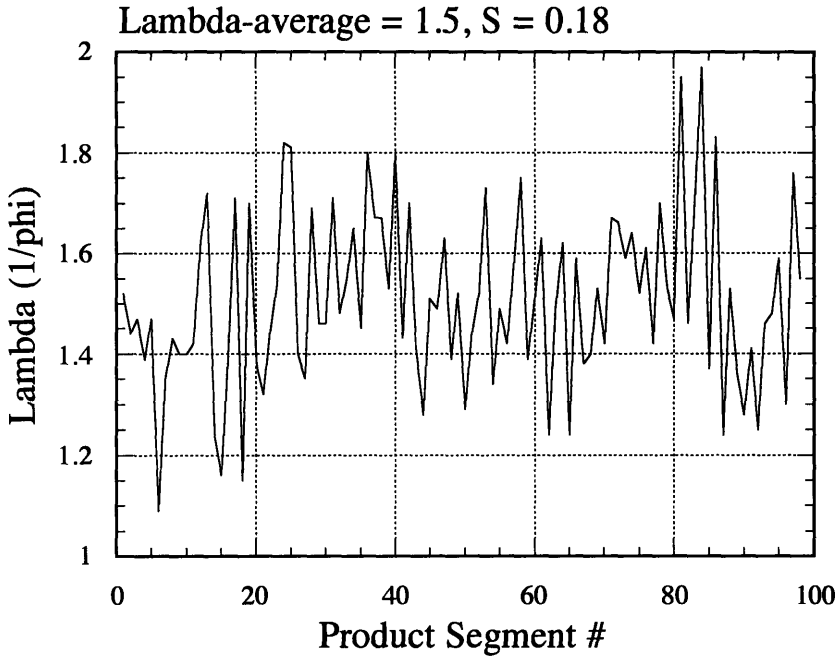

Figure 4.16 Typical Phi history for a distributed case.

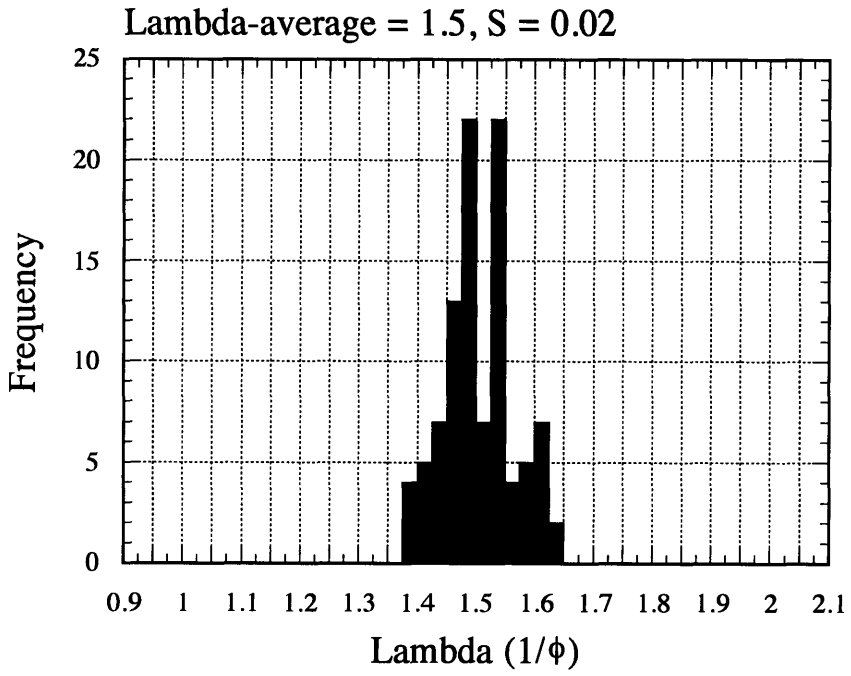

Figure 4.17 Phi profile for s = 0.02

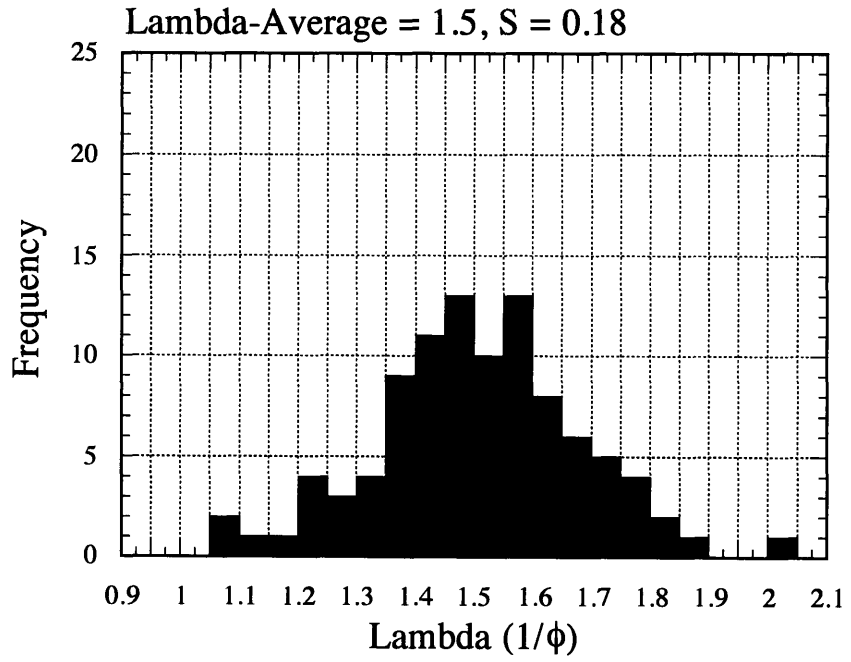

Figure 4.18 Phi profile for s = 0.18

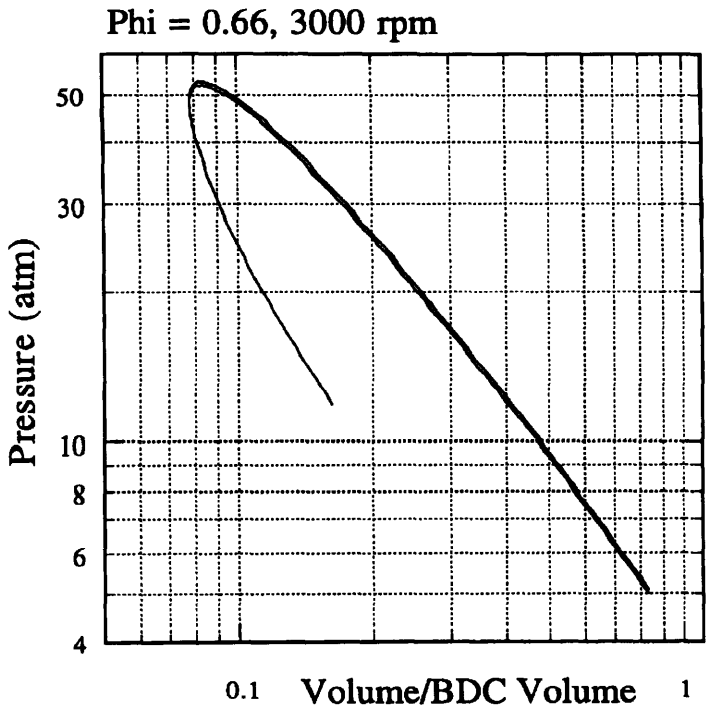

Figure 4.19 Pressure-Volume traces showing the agreement between the distributed and non-distributed cases.

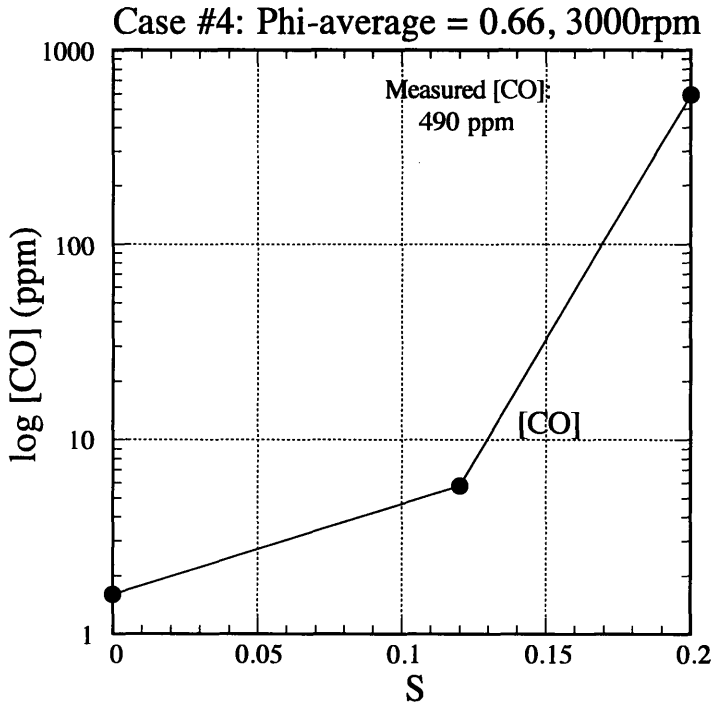

Figure 4.20 CO emissions versus S for case #4.

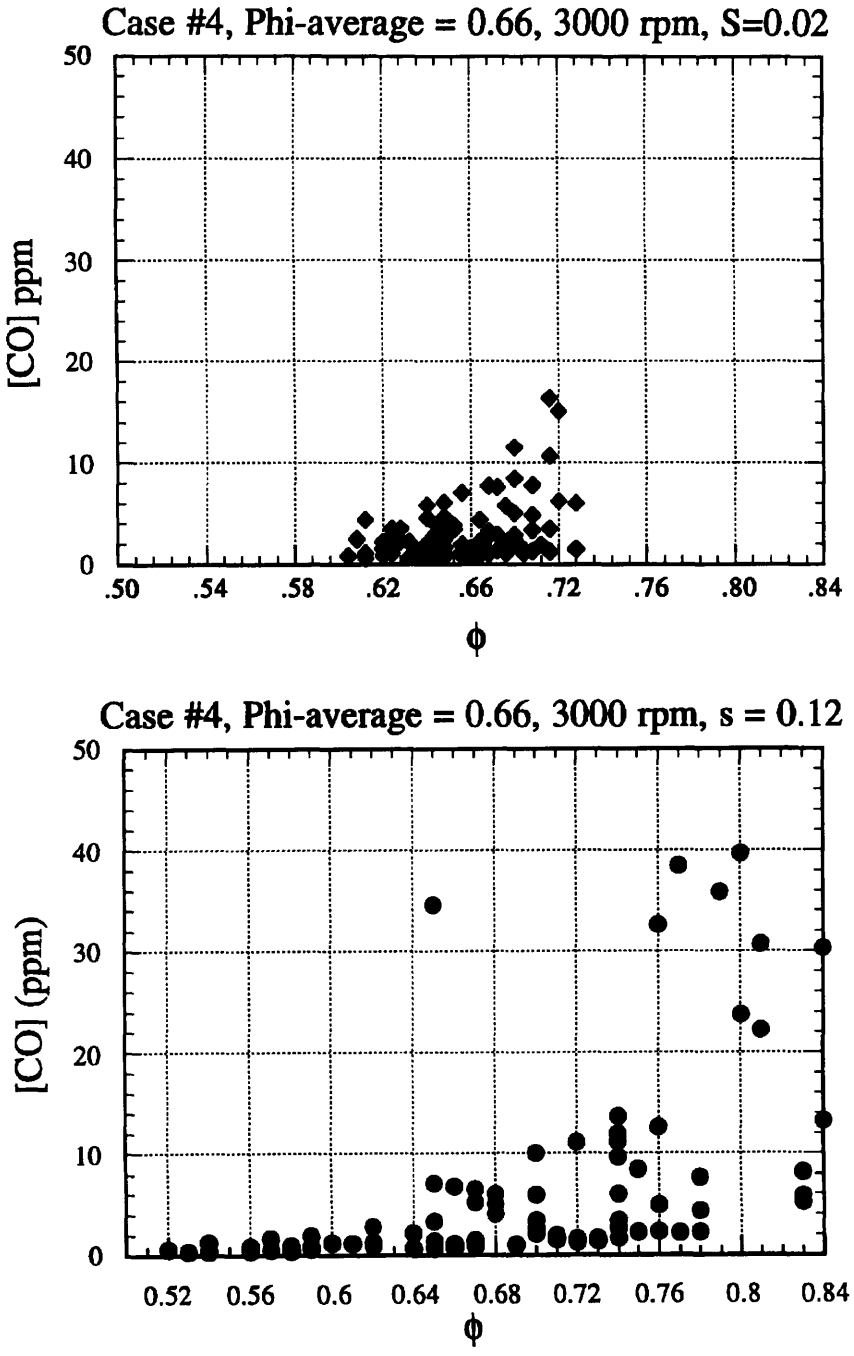

Figures 4.21 and 4.22 CO concentration in each product element plotted against its initial phi, for two different unmixidness levels.

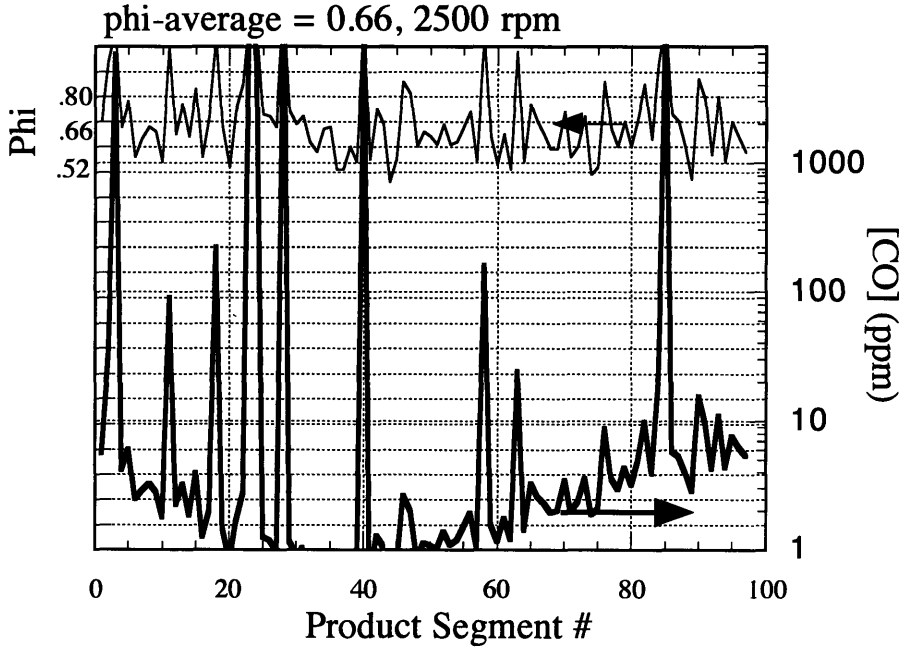

Figure 4.23 CO for each segment plotted alongside the phi for that segment, showing that rich segments dominate in CO contribution, especially towards the late segments.

5. Conclusions

Predicting emissions for small engines running at high speeds and burning lean mixtures poses specific demands on the modeling effort. All of these operating conditions affect the time scales of the dominant and interdependent pressure, temperature and chemical processes and increase the probability for non equilibrium behaviors to affect the dominant emissions mechanisms. Looking at these conditions a priori, there was motivation to build the emissions model with detailed chemical kinetic capabilities around a simple zero dimensional thermodynamic model of the engine cycle. While the discrete nature of the cycle calculations introduce errors in the thermodynamic calculations, the accuracy of the kinetics let other issues be explored. In looking at much of the results, building COOK with a detailed kinetics capability was probably not essential in most of these cases since even while engine speeds were much higher than most previous modeling studies, the temperatures present under these conditions were well within the regime for equilibrium assumptions to hold. In many other modeling work, steady state assumptions are made for some of the intermediates like N. COOK's studies do support these assumptions in a general sense. For example, figure 2.5 shows the N concentration throughout the cycle to be more than 3 orders of magnitude less than that of other important radicals in the NO formation mechanism.

Previous NO modeling had focused on making predictions and delineating factors affecting NO emissions. Examining the modeling issues behind these predictions in more detail can shed a light on the nature of NO modeling, the realistic NO formation processes, as well as possible strategies for emissions reduction. The results of the modeling show that NO emissions could be predicted with good accuracy for a range of experimental cases. Here it was shown that the formation time dominates lean NO formation and almost any strategy to shorten that time will have an impact on NO emissions. Efficiency is also affected as shorter burn times are more efficient but can also yield very high NO emissions resulting from the generally higher peak temperatures. Lean operation is affected greatly by combustion stability, as much of the combustion phase is closer to its lean operating limit and any substantial combustion instability is unacceptable for operation and will lower efficiency. Keeping the balance between smooth operation and very lean mixtures via high turbulence levels and fast burning would lower NO emissions substantially. The limitations in

COOK prevented useful modeling of the effects of heat loss, crevice and wall interactions and quenching. Since NO is formed mainly in the core of the cylinder among the hotter and earlier burned elements, as verified by both COOK's predictions and experimentally [7], these missing phenomena did not affect substantially the NO emissions calculations. This is diametric to the case for CO emissions calculations.

CO emissions are dominated by wall phenomena not included in the fundamental framework of the COOK model. This absence, however, let its significance be analyzed by looking at the discrepancy between the model and the experimental data. Experimental data clearly show that the dominant HC emissions mechanisms also seem to influence CO emissions to a similar degree. The mechanisms: wall quenching, and possibly crevice interactions have different effects on mixtures of different fuel air ratios and the differences between the model and the experimental results help to illustrate them. The rich mixtures, for example, should be effected in similar ways by wall interactions as the lean mixtures since both operate at lower temperatures and are equally close to an unstable combustion limit. The range of data introduced in Heywood show how the predictions' errors grow as the dominant wall behaviors become more important away from stoichiometric. Modeling of lean CO emissions should place major effort on the wall interactions, and much less on the detailed calculation of the properties of the bulk gases.

The use of a model like COOK could be expanded to other emissions like hydrocarbon or soot given more detailed combustion modeling. The use of full kinetics gives flexibility as to the level of detail in the model and can help to study subtleties of the post combustion process like radical recombination or other nonequilibrium phenomena important to understanding emissions processes. This flexibility is by far the most novel aspect behind COOK's construction and can prove to be very important in investigating more and varied chemical processes in engines. Given newer and more complex mechanisms, Grimech 2.11 for example, the significance of different reaction pathways, rates, and intermediates can be determined. These calculations can show the importance of both the chemical aspects in the modeling but potential real life modifications which could prove to be important to the behavior of the system and for modifying the emissions characteristics. In conjunction with the more advanced chemical mechanisms and the continual exploration for new and cleaner fuels and operating conditions, COOK could be a very useful tool in modeling future engine developments.

Appendix A: Methmech methane combustion mechanism.

The output from the Chemkin interpreter lists the reactions included in the kinetics for the Methmech input.

CHEMKIN INTERPRETER OUTPUT:

(k = A T**b exp(-E/RT))

REACTIONS	A	b	E
1. CH3+H+M=CH4+M	8.00E+26	-3.0	0.0
2. CH4+O2=CH3+HO2	7.90E+13	0.0	56000.0
3. CH4+H=CH3+H2	2.20E+04	3.0	8750.0
4. CH4+O=CH3+OH	1.60E+06	2.4	7400.0
5. CH4+OH=CH3+H2O	1.60E+06	2.1	2460.0
6. CH3+O=CH2O+H	6.80E+13	0.0	0.0
7. CH3+OH=CH2O+H2	1.00E+12	0.0	0.0
8. CH3+OH=CH2+H2O	1.50E+13	0.0	5000.0
9. CH3+H=CH2+H2	9.00E+13	0.0	15100.0
10. CH2+H=CH+H2	1.40E+19	-2.0	0.0
11. CH2+OH=CH2O+H	2.50E+13	0.0	0.0
12. CH2+OH=CH+H2O	4.50E+13	0.0	3000.0
13. CH+O2=HCO+O	3.30E+13	0.0	0.0
14. CH+O=CO+H	5.70E+13	0.0	0.0
15. CH+OH=HCO+H	3.00E+13	0.0	0.0
16. CH+CO2=HCO+CO	3.40E+12	0.0	690.0
17. CH2+CO2=CH2O+CO	1.10E+11	0.0	1000.0
18. CH2+O=CO+H+H	3.00E+13	0.0	0.0
19. CH2+O=CO+H2	5.00E+13	0.0	0.0
20. CH2+O2=CO2+H+H	1.60E+12	0.0	1000.0
21. CH2+O2=CH2O+O	5.00E+13	0.0	9000.0
22. CH2+O2=CO2+H2	6.90E+11	0.0	500.0
23. CH2+O2=CO+H2O	1.90E+10	0.0	-1000.0
24. CH2+O2=CO+OH+H	8.60E+10	0.0	-500.0
25. CH2+O2=HCO+OH	4.30E+10	0.0	-500.0
26. CH2O+OH=HCO+H2O	3.43E+09	1.2	-447.0
27. CH2O+H=HCO+H2	2.19E+08	1.8	3000.0
28. CH2O+M=HCO+H+M	3.31E+16	0.0	81000.0
29. CH2O+O=HCO+OH	1.81E+13	0.0	3082.0
30. HCO+OH=CO+H2O	5.00E+12	0.0	0.0
31. HCO+M=H+CO+M	1.60E+14	0.0	14700.0
32. HCO+H=CO+H2	4.00E+13	0.0	0.0
33. HCO+O=CO2+H	1.00E+13	0.0	0.0
34. HCO+O2=HO2+CO	3.30E+13	-0.4	0.0
35. CO+O+M=CO2+M	3.20E+13	0.0	-4200.0
36. CO+OH=CO2+H	1.51E+07	1.3	-758.0
37. CO+O2=CO2+O	1.60E+13	0.0	41000.0
38. HO2+CO=CO2+OH	5.80E+13	0.0	22934.0
39. H2+O2=2OH	1.70E+13	0.0	47780.0
40. OH+H2=H2O+H	1.17E+09	1.3	3626.0
41. H+O2=OH+O	5.13E+16	-0.8	16507.0

42. O+H2=OH+H			1.80E+10	1.0	8826.0
43. H+O2+M=HO2+M			3.61E+17	-0.7	0.0
H2O	Enhanced by	1.860E+01			
CO2	Enhanced by	4.200E+00			
H2	Enhanced by	2.860E+00			
CO	Enhanced by	2.110E+00			
N2	Enhanced by	1.260E+00			
44. OH+HO2=H2O+O2			7.50E+12	0.0	0.0
45. H+HO2=2OH			1.40E+14	0.0	1073.0
46. O+HO2=O2+OH			1.40E+13	0.0	1073.0
47. 2OH=O+H2O			6.00E+08	1.3	0.0
48. H+H+M=H2+M			1.00E+18	-1.0	0.0
49. H+H+H2=H2+H2			9.20E+16	-0.6	0.0
50. H+H+H2O=H2+H2O			6.00E+19	-1.2	0.0
51. H+H+CO2=H2+CO2			5.49E+20	-2.0	0.0
52. H+OH+M=H2O+M			1.60E+22	-2.0	0.0
H2O	Enhanced by	5.000E+00			
53. H+O+M=OH+M			6.20E+16	-0.6	0.0
H2O	Enhanced by	5.000E+00			
54. H+HO2=H2+O2			1.25E+13	0.0	0.0
55. HO2+HO2=H2O2+O2			2.00E+12	0.0	0.0
56. H2O2+M=OH+OH+M			1.30E+17	0.0	45500.0
57. H2O2+H=HO2+H2			1.60E+12	0.0	3800.0
58. H2O2+OH=H2O+HO2			1.00E+13	0.0	1800.0
59. N2+O=>NO+N			1.80E+14	0.0	76241.2
60. NO+N=>N2+O			3.80E+13	0.0	844.5
61. N+O2=>NO+O			1.80E+10	1.0	9299.2
62. NO+O=>N+O2			3.80E+09	1.0	41369.3
63. N+OH=>NO+H			7.10E+13	0.0	894.1
64. NO+H=>N+OH			1.70E+14	0.0	48800.7

NOTE: A units mole-cm-sec-K, E units cal/mole

Appendix B: A Marxist view of air pollution

Air pollution is as much a result of chemical processes as it is economic ones. Pollution and environmental degradation result from two main socio-economic mechanisms: an unplanned, competitive economy and an hierarchical social structure.

Hierarchical societies will and always have subjected their exploited classes to lower living and working conditions. Today's world can be divided into the capitalist class and its apparatus, and the working class, which includes a substantial middle class. The 'lower' working class, located mainly in Africa, Asia and Latin America, but also in pockets within every country in the world, deals with the brunt of the social production. Hundreds of millions live, work and die in mines, oil fields, mills, factories, lumber yards, plantations and other places where extreme and brutal environmental factors affecting health and longevity take their toll. The working class is the fodder of capitalism, hierarchically, the bottom, and it's among the working classes where health risks like air pollution are commonplace. The middle class, which makes up substantially places like Europe and North America have been sheltered, comparably, from extreme environmental contamination mainly because of the Capitalist class' need for political stability and coercion to maintain the major consumption sink which is the middle class. Exemplifying these hierarchical relationships are things like DDT which, though, banned for use in the United States, is still manufactured (by U.S. companies) for pesticide use in Asia and Latin America. Moving factories to poor countries with lower environmental standards is reported daily in any of the business press, a clear manifestation of the stratified nature of society.

Unplanned, competitive economies are prone to faults like pollution, thermodynamic waste, resource depletion and general environmental degradation. Under capitalism goods are produced based on their profit potential, not use. This competitive system tends to leave unchecked things like waste and pollution since they are rarely reflected in prices. Since costs lower profits, and lower profits will eliminate a firm from competition, any costs incurred in treating waste or lowering pollution must be minimized. The Capitalist class manipulates culture through its media and political entourage, creating the demand for products otherwise not needed, which depletes resources and increases pollution. The manipulation of culture by the auto industry, mentioned in chapter one, is good example of this. Hundreds of times the numbers of cars actually needed are produced and forced onto the market via billions of dollars in advertising, lobbying, policy and political manipulation. The result is the depletion of oil and metal resources around the world and the pollution of the air in every major city in the world. Pulp and paper manufacturers as well have been implicated in creating useless markets to stimulate demand for large amounts of paper,

destroying forests around the world.

Planning an economy around use and not around profit is the only long term solution to curbing environmental degradation and resource depletion. Eliminating private property and commercial information sources are essentials as well in revolutionizing the way humans relate to the earth, the way in which nature is put to use economically for human needs and for making human society sustainable for hundreds of generations to come.

References

1. Raine, R. R. et al. Combustion and flame **102**, 241, 1995.
2. Daneshyar, H, et al Combustion and Flame **21**, 395, 1973.
3. Newhall, H. 12th International Symposium on Combustion, 603, 1968.
4. Aiman, W. 14th International Symposium on Combustion, 861, 1972.
5. Komiyama, K. et al SAE paper 730475, 1973.
6. Heywood, J. B., Higginis, et al SAE paper 790291, 1979.
7. Lavioe, G., Heywood, J. B. et al. Combustion Science and Technology, **1**, 313, 1970.
8. Keck, J. C. et al Combustion and Flame **17**, 237, 1971.
9. Delichatsios, M. MIT Dept of Mech Eng S.M. Thesis, 1972.
10. Gad El-Mawla, A., et al U. Michigan PhD Thesis, 1965.
11. Heywood, J. B. Internal Combustion Engine Fundamentals, McGraw Hill, New York, 1988.
12. Kee, R., et al. Sandia Report 89-8009, 1989.
13. Lutz, A., et al, Sandia Report 87-8248, 1987.
14. Wellburn, A., Air Pollution and Climate Change, Longman Scientific and Technical, New York, 1994.
15. Ramos, J., Internal Combustion Engine Modeling, Hemisphere, New York, 1989.
16. Foster, J., The Venerable Planet, Cornerstone Books, New York, 1994.
17. Seager, J., The New State of the World Atlas, Simon and Schuster, New York, 1995.
18. Smil, V. Energy in World History, Westview Press, Boulder, CO, 1994.
19. Committe on Medical and Biological Effects of Environmental Pollutants, Vapor Phase Organic Pollutants, 1976.
20. Committee on Medical and Biological Effects of Environmental Pollutants, Nitrogen Oxides, 1977.
21. Goudie, A., Human Impact on the Natural Environment, Blackwell, Cambridge, Ma, 1993.
22. Heywood, J., 14th International Symposium on Combustion, 1972.
23. Blumberg, P, et al, Combustion Science and Technology, **4**, 73, 1971.
24. Fergusen, C., Internal Combustion Engines, Wiley and Sons, New York, 1986.

25. Stone, R. Introduction to Internal Combustion Engines, 2nd Ed, Macmillan, Basingstoke, 1992.

26. Miller, J. A.and Bowman, C. T.. Mechanism and Modeling of Nitrogen Chemistry in Combustion. Progress in Engineering Combustion and Science, **15**, 287, 1989.

27. Van Wylen, 0. Fundamentals of Classical Thermodynamics, 1986.

28. Thijssen, J. H. MIT Dept of Chemical Engineering PhD thesis, 1993.

29. Taylor, C., The Internal Combustion Engine in Theory and Practice, MIT press, Cambridge, 1985.

30. Borman, G. and Kazuie Nishiwaaki. Internal Combustion Engine Heat Transfer. Progress in Energy and Combustion Science, **13**, 1, 1987.

31. Steinfeld, J.I. et al Chemical Kinetics and Dynamics, Prentice Hall, New Jersey, 1989.

32. Turk, S.L. MIT Dept of Mechanical Engineering S.M. Thesis, 1972

33. Flagan, R.C. et al Fundamentals of Air Pollution Engineering, Prentice Hall, New Jersey, 1988

34. Hanson, R. K. et al Combustion Chemistry (Gardener, W. ed.) p361-421, 1989.

35. Olsen, M. Race Poverty and the Environment **6**, 1995.

36. Lewis, H. With Every Breath You Take, Crown, New York, 1965

37. Poulos, S. G, et al SAE paper 830334, 1983

38. Bowman, C. T.. 24Th International Symposium on Combustion, 859-878, 1992.

39. Glarborg, P., Miller, J. A.. et al.. Combustion and Flame **65**:177-202, 1986

3961-36